공학박사 학위논문

General relativistic effects on geometric phase evolution of a photon state

일반 상대론적 효과에 의한 광자의 기하학적 위상 변화

2023 년 2 월

서울대학교 대학원

전기정보공학부

노한솔

General relativistic effects on geometric phase evolution of a photon state

지도 교수 박남규

이 논문을 공학박사 학위논문으로 제출함
2023년 02월

서울대학교 대학원
전기정보공학부
노한솔

노한솔의 공학박사 학위논문을 인준함
2023년 02월

위 원 장 오 정 석 (인)

부위원장 박 남 규 (인)

위 원 안 도 열 (인)

위 원 김 기 홍 (인)

위 원 유 선 규 (인)

Abstract

General relativistic effects on geometric phase evolution of a photon state

With recent advancements of free-space quantum optical systems consisting of satellites, the investigation of the evolution of photon states in gravitational field has been widely studied but mostly confined to the study of proper time. While there are also a few works about the effects from local frames on quantum photon states, called Wigner rotation, it has been interpreted as the Berry phase of classical polarization vectors along a photon trajectory. Here, the Wigner rotation is investigated to study geometric phases induced by Earth's gravitational field for observers in various orbits. It is found that a potentially measurable phase of the Wigner rotation angle in addition to the rotation of standard fame, the latter of which is computed and agrees well with the geodetic rotation. When an observer is in either a circular orbit containing non-zero angular momentum, the additional phase contributes 10^{-6} degree to 10^{-4} degree respectively, depending on the altitude of the Earth orbit. In the former case, the additional phase is dominant over the near-zero classical geodetic rotation. This shows that the Wigner rotation represents a non-trivial semi-classical effect of quantum field theory on a background classical gravitational field.

It is also shown that coincidence rates in two-photon astronomical quantum

interferometry consisting of satellites on polar orbits near Earth can be variated in combination with pure quantum optical effect, Hong-Ou-Mandel dip, owing to the relatively large non-trivial geometric phase differences between the photon trajectories with the positive and negative velocity component in the direction of the quantization axis.

Keyword : Wigner rotation, astronomical interferometer, Quantum key distribution, Hong-Ou-Mandel effect

Student Number : 2017-31651

Table of Contents

List of Tables

List of Figures

Chapter 1. Introduction

1.1. Study Background

Quantum optical technologies have shown their supremacy in many applications of secure communications and sophisticated measurements. Taking advantage of the intrinsic immunity of quantum communications to tampering and eavesdropping, various quantum communication protocols have been widely studied using not only optical fiber but also satellites and ground stations with the recent deployment of the Quantum Experiments at Space Scale network and Micius satellite[1-20]. Using tailored photons as input states, quantum interferometry have also been reported to overcome the classical limit of interferometry sensitivity, O($1/\sqrt{N}$), up to the intrinsic Heisenberg limit, O($1/N$), which corresponds to an eight-order-of-magnitude improvement of SNR in milliwatts-optical-laser interferometers[21]. The quantum optical interferometry has its potential applications in elaborate satellite-based metrology systems[21] such as the European Laser Interferometer Space Antenna (LISA) for the detection of gravitational wave.

One of the big challenges in these quantum optical systems with satellites is the determination of phase variations induced by gravitational rotations on both satellites and photon states along the geodesics. Accordingly, synchronization of polarization reference-frame and evolutions of the photon states should be considered for free-space QKD systems[22] and

quantum optical interferometry based on satellites[23] in the gravitational field[23] which induces the de Sitter (geodetic precession) effects[24].

Therefore, it is important in these environments to understand the interplay of quantum theory and gravitation as the photon state, propagating between the ground station and the satellite, carries the quantum information. While the gravitational field is known to add a measurable contribution to the quantum bit error rate (QBER) along the worldline of the quantum state as the altitude changes[20] in addition to the red shift[25,26], the experiment regimes of several proposals suggested for quantum communication between a LEO satellite and an optical ground station, such as SPACEQEST and QEYSSAt projects, have not fully assessed evolution of quantum states induced in curved space-time; most of them have mainly considered quantum optics rather than general relativistic phenomena of quantum states at large scales[17-20].

In addition to the geodetic precession, the spin angular momentum of an astronomical body has been reported to have other extraordinary phenomena such as the Penrose process in the ergosphere[27], chaotic geodesics[28], and the additional gravitational precession, the Lense-Thirring (frame-dragging) effect[24,29-31]. Especially, the frame-dragging effects dictate different phase-variations of photons near a Kerr black hole along their worldlines in a combination with the geodetic precession and redshift, leading to geometrically-induced unique Orbital Angular Momentum (OAM) profiles

in the sky of an asymptotic observer[32]. Moreover, it has been reported that Sagnac effects from the rotational frame-dragging can variate the coincident rates of two photon states in a Hong–Ou–Mandel (HOM) interferometer surrounding a spinning astronomical object[33]; the two single photons travel on clockwise and anticlockwise half of circular paths respectively and then enter into a 50:50 beam splitter in the opposite. The Sagnac effects result in measurable variation of the coincident rates around a Kerr blackhole, but not near Earth due to its relatively low spinning angular momentum and weak gravitational field.

Describing photon states observed by a moving observer (e.g., a satellite) in curved spacetime requires the understanding of both quantum mechanics and general relativity, two essential branches of modern physics. One of the conceptual barriers for the relativistic treatment of quantum information is the difference in the role played by the wave fields and the state vectors in relativistic quantum theory. In non-relativistic quantum mechanics, the wave function of the Schrödinger's equation gives the probability amplitude that can be used to define conserved particle densities or density matrices. However, it was discovered that relativistic equations are only indirect representations for probability waves of a single particle[34]. In 1939, Wigner proposed the idea that the quantum states of relativistic particles can be formulated without the use of wave equations[35]. He showed that the states of a free particle are given by a unitary irreducible representation of the

Poincaré group. In Wigner's formulation, relativistic-particle states in different inertial frames are related by a little group element in the irreducible representation of the Poincaré group, called Wigner rotation[34-42].

While Wigner's original proposal was for special relativity, there have been several attempts to extend it to the domain of general relativity[39-42]. It has been shown that moving-particle states in curved spacetime are transformed into each other by Wigner rotation[39-42] by introducing tetrads (frame fields) to define local coordinates[43] since extending Wigner's group to curved spacetime requires the standard local laboratory at every event[44].

1.2. Purpose of Research

In this work, we investigate the effects on WRAs from the spinning angular momentum of gravitating object (J) axial angular momentums of photon (l_{photon}) by calculating WRAs along representative photon trajectories on the equatorial plane with different positive and negative angular momentums l_{photon} for two types of circular orbits, equatorial and polar orbits. It is demonstrated that WRAs depend on the two angular momentums, J and l_{photon} by calculating WRAs for observers' frames on a thin accretion disk of a supermassive blackhole, for example, M87 with and without the spinning angular momentum J for various photon angular momentums l_{photon}. For Earth, while its small spinning angular momentum J does not add any additional phase to the WRAs up to order of 10^{-8} as assumed in many previous works[45,46] and angular momentum of photon geodesics l_{photon}

changes only a minute amount of geodetic precession contribution (10^{-8}~10^{-14}) for observers' frames whose quantization axis are orthogonal to the equatorial plane, different sign of l_{photon} leads to measurable differences of residual phases in WRA for observers in the frame where the quantization axis and photons lie on the same plane. Utilizing the dependence of WRA on sign of l_{photon}, we introduce an 'astronomical' Mach-Zehnder interferometer near Earth with an indistinguishable two-photon input state travelling along one of arms in combination with HOM effect; the two photon states simultaneously entering into the first beam splitter, one in each port, becomes a superposition of two-photon states emitting into each arm, as known as HOM effect. Along one of the arms, the photon state is sent to the second beam splitter in the satellites on a polar orbit after which the coincidence rates are measured. The relative WRA difference between two photon states in one of two arms variates the coincidence rates. This finding is distinguished from the features of classical interferometry since it stems from the pure quantum interferometry characteristics, HOM effect. We believe these results could provide a potential testbed of the interplay of general relativity and quantum theory.

Chapter 2. Lorentz transformation and Wigner rotation in curved spacetime

In 1939, Wigner classified that quantum states of a free particle with the Poincaré group by introducing a subgroup of the Lorentz group, called the little group, which has finite unitary irreducible representations; in this formalism, arbitrary Lorentz transformation results in additional phases of photon states, called the Wigner rotation angles (WRAs)[34-42]. This Wigner's representation can be extended to a general relativistic framework by applying Einstein's equivalence principle and local orthonormal bases known as tetrads[43]. The transformations of local frames (tetrads) between two events of observers can be seen as local Lorentz transformations and naturally represented by the Wigner rotation[39-42]. In this chapter, the details of derivation of WRAs are shown in terms of infinitesimal Lorentz transformations. Then, physical meanings of WRAs for linear- and circular-polarized photon states are given.

2.1. Irreducible representation of the Wigner rotation in curved spacetime

The Hilbert space vector of a photon is defined in a local inertial frame spanned by a tetrad, $e_{\hat{a}}{}^{\mu}(\mathbf{x})$, $\hat{a}$ and μ = 0, 1, 2, 3, which satisfies $g_{\mu\nu}(\mathbf{x}) = \eta_{\hat{a}\hat{b}} e^{\hat{a}}{}_{\mu}(\mathbf{x}) e^{\hat{b}}{}_{\nu}(\mathbf{x})$ and transforms in a way that $\overline{e}_{\hat{a}}{}^{\mu}(\overline{\mathbf{x}}) = \frac{\partial \overline{x}^{\mu}}{\partial x^{\nu}} e_{\hat{a}}{}^{\nu}(\mathbf{x})$ and $\overline{e}_{\hat{a}}{}^{\mu}(\mathbf{x}) = \Lambda_{\hat{a}}{}^{\hat{b}} e_{\hat{b}}{}^{\mu}(\mathbf{x})$ under general coordinate and local Lorentz transformations, respectively. Throughout the paper, we use hatted Latin letters for local inertial coordinates and Greek letters for general coordinates. The tetrad $e_{\hat{a}}{}^{\mu}(\mathbf{x})$ carries two indices: (i) a "world index" μ that transforms under general coordinate transformations of general relativity, and (ii) a local tangent plane index $\hat{a}$ which transforms under local, **x**-dependent Lorentz transformation $\Lambda(\mathbf{x})$. Quantities such as $p_{\hat{a}}(\mathbf{x}) = e_{\hat{a}}{}^{\mu}(\mathbf{x}) p_{\mu}(\mathbf{x})$ are the projection of the general relativistic world momentum vector $p_{\mu}(\mathbf{x})$ onto the axes (three spatial, one temporal) of the observer's local laboratory frame[47] where the metric is locally flat such that special relativity holds over distances over which the curvature can be considered as essentially constant. The tetrad, therefore, explicitly embodies Einstein's Equivalence Principle through the index $\hat{a}$. The local Lorentz transformation $\Lambda_{\hat{b}}{}^{\hat{a}}(\mathbf{x})$ transforms between different instantaneous states of motion of the observer (e.g.

stationary, freely-falling, circular motion, or arbitrary motion) within the *same* Lorentz tangent plane at the position **x** , i.e. the tetrad is constructed to define (and describes) the observer's instantaneous state of motion at each point **x.**

A variation of a tetrad under an infinitesimal translation from **x** to **x** +δ**x** is described by parallel transport to compare two vectors in the same tangent plane without a change of the vectors such that[38,48]

$$\delta\left(e_{\hat{a}}{}^{\mu}\right)=\overline{e}_{\bar{a}}{}^{\mu}(\mathbf{x}+\delta\mathbf{x})-\overline{e}_{\hat{a}}{}^{\mu}(x)\rightarrow\delta x^{\lambda}\nabla_{\lambda}e_{\hat{a}}{}^{\mu}(\mathbf{x})\,. \tag{1}$$

For the case that wave vector of a photon is measured in the observer's laboratory, local covariant components of the wave vector, $k_{\hat{a}}(\mathbf{x})=e_{\hat{a}}{}^{\mu}(\mathbf{x})k_{\mu}(\mathbf{x})$, are changed along the photon's geodesic from x^{μ} to $x^{\mu}+k^{\mu}(\mathbf{x})\delta\xi$ such that

$$\delta k_{\hat{a}}(\mathbf{x})=\delta\left(e_{\hat{a}}{}^{\mu}(\mathbf{x})\right)k_{\mu}(\mathbf{x})+e_{\hat{a}}{}^{\mu}(\mathbf{x})\delta k_{\mu}(\mathbf{x})\,;\ \delta k_{\mu}(\mathbf{x})=d\xi\nabla_{\mathbf{k}}k_{\mu}(\mathbf{x})\,. \tag{2}$$

Since a photon state in curved spacetime follows a null geodesic in the geometric optics limit[49] and under a local infinitesimal change of a tetrad (which is antisymmetric[38,39]), Eq. (2) can be rewritten as

$$k_{\hat{a}}(x)\rightarrow k'_{\hat{a}}(x)\equiv k_{\hat{a}}(\mathbf{x})+\delta k_{\hat{a}}(\mathbf{x})=\left(\delta_{\hat{a}}{}^{\hat{b}}+\lambda_{\hat{a}}{}^{\hat{b}}(\mathbf{x})d\xi\right)k_{\hat{b}}(\mathbf{x})=\Lambda_{\hat{a}}{}^{\hat{b}}(\mathbf{x})k_{\hat{b}}(\mathbf{x}) \tag{3}$$

where $\lambda_{\hat{a}}{}^{\hat{b}}(\mathbf{x})=\left(\nabla_{\mathbf{k}}e_{\hat{a}}{}^{\nu}(\mathbf{x})\right)e_{\nu}{}^{\hat{b}}(\mathbf{x})$. In other words, the effect of an infinitesimal translation can be considered as an infinitesimal local Lorentz

transformation given by $\Lambda_{\hat{a}}{}^{\hat{b}}(\mathbf{x}) = \delta_{\hat{a}}{}^{\hat{b}} + \lambda_{\hat{a}}{}^{\hat{b}}(\mathbf{x})$ [38,39,41,42].

A Lorentz transformation, Λ, has the one-dimensional representations for a photon state with the helicity, σ, given by[36]

$$U(\Lambda)\left|\mathbf{k},\sigma\right\rangle = \sum_{\sigma'} D_{\sigma'\sigma}\left(W(\Lambda,\mathbf{k})\right)\left|\Lambda\mathbf{k},\sigma'\right\rangle . \tag{4}$$

$W(\Lambda,\ \mathbf{k})$ is the Wigner's little group element, defined as $W(\Lambda,\mathbf{k}) = L^{-1}(\Lambda\mathbf{k})\,\Lambda L(\mathbf{k})$ and $D(W)$ is the irreducible representation of W. $L(\mathbf{k})$ is the Lorentz transformation such that $L(\mathbf{p})\mathbf{k} = \mathbf{p}$. Accordingly, a displacement of a photon state leads to a residual phase called the Wigner rotation angle (WRA). To get an explicit expression of the irreducible unitary representation of a Lorentz transformation, we use the canonical group homomorphism between the proper Lorentz group and its double cover, $SL(2, \mathbb{C})$; a wave vector $\mathbf{k}$ of a photon is mapped to a Hermitian matrix K via $K = \sigma_{\hat{a}} k^{\hat{a}}$, where $\sigma_{\hat{a}}$, $\hat{a}$ = 1, 2, and 3, are the Pauli matrices, and $\sigma_{\hat{0}}$ is the 2x2 identity matrix. A Lorentz transformation is represented by the similarity transformation such that

$$AKA^{\dagger} = \Lambda^{\mu}{}_{\nu} k^{\nu} \sigma_{\mu} \tag{5}$$

with an element $A = \begin{pmatrix} \alpha & \beta \\ \gamma & \delta \end{pmatrix}$ of $SL(2, \mathbb{C})$. For an infinitesimal homogeneous Lorentz, the matrix A can be expanded in terms of $d\xi$ such that

$$A=\begin{pmatrix}\alpha & \beta\\ \gamma & \delta\end{pmatrix}=I+\tilde{A}d\xi=I+\begin{pmatrix}\tilde{\alpha} & \tilde{\beta}\\ \tilde{\gamma} & -\tilde{\alpha}\end{pmatrix}d\xi\,. \tag{6}$$

Substituting Eq. (6) into Eq. (5), multiplying $\sigma_{\hat{a}}$ both sides, and then taking a trace on both sides, we can get the following equations

$$\lambda^{\hat{a}}{}_{\hat{b}}=\frac{1}{2}\delta^{\hat{a}\hat{c}}tr(\sigma_{\hat{b}}\sigma_{\hat{c}}\tilde{A}+\sigma_{\hat{c}}\sigma_{\hat{b}}\tilde{A}^{\dagger})\,, \tag{7}$$

where tr(A) is the trace of A. That is, we obtain $\tilde{\alpha}$, $\tilde{\beta}$, and $\tilde{\gamma}$ in terms of $\lambda^{\hat{a}}{}_{\hat{b}}$ such that

$$\begin{aligned}\tilde{\alpha}&=\frac{1}{2}(\lambda^{\hat{0}}{}_{\hat{3}}+\mathrm{i}\,\lambda^{\hat{1}}{}_{\hat{2}})\\ \tilde{\beta}&=\frac{1}{2}[(\lambda^{\hat{0}}{}_{\hat{1}}+\lambda^{\hat{3}}{}_{\hat{1}})+\mathrm{i}(-\lambda^{\hat{0}}{}_{\hat{2}}+\lambda^{\hat{2}}{}_{\hat{3}})]\\ \tilde{\gamma}&=\frac{1}{2}[(\lambda^{\hat{0}}{}_{\hat{1}}-\lambda^{\hat{3}}{}_{\hat{1}})+\mathrm{i}(\lambda^{\hat{0}}{}_{\hat{2}}+\lambda^{\hat{2}}{}_{\hat{3}})].\end{aligned} \tag{8}$$

The corresponding irreducible unitary representation of the little group element for a massless particle is[42,50]

$$\mathrm{e}^{\mathrm{i}(\psi(\Lambda,\mathrm{k})/2)}=\frac{[\alpha(1+\mathrm{n}^{\hat{3}})+\beta\,\mathrm{n}_{+}]\mathrm{b}+[\gamma(1+\mathrm{n}^{\hat{3}})+\delta\,\mathrm{n}_{+}]\mathrm{c}^{*}}{a\sqrt{b(1+\mathrm{n}^{\hat{3}})}}\,, \tag{9}$$

where $\Psi(\Lambda,\,\mathbf{k})$ is the WRA. Detailed expressions for *a*, *b*, *c*, and *d* are given in the Appendix. Thus, a local infinitesimal Lorentz transformation $\Lambda(\mathbf{x})$ leads to an infinitesimal Wigner rotation angle (IWRA) $\tilde{\psi}$, and the total Wigner rotation angle ψ can be formally obtained by a time-ordered integration of IWRs over the geodesic trajectory $\mathbf{x}(\xi)$ of the photon such that

$$\mathrm{e}^{\mathrm{i}\psi(\Lambda,\vec{n})} = T\exp\left[\mathrm{i}\int\tilde{\psi}(\Lambda(\mathbf{x}(\xi)),n^{\hat{i}}(\xi))d\xi\right], \tag{10}$$

where $n^{\hat{i}} = k^{\hat{i}}(\mathbf{x})/k^{\hat{0}}(\mathbf{x})$, and T is the time-ordering operator.

2.2. Wigner rotation on linear- and circular-polarized photon states

Under a Lorentz transformation Λ, a polarization vector, $e^{\mu}_{\sigma}(\hat{\mathbf{k}},\sigma)$ of a photon field, is transformed as[36]

$$\begin{aligned} &M(\Lambda)^{\hat{a}}{}_{\hat{b}}\, e^{\hat{b}}_{\sigma}(\hat{\mathbf{k}},\sigma) = \sqrt{\frac{k^{\hat{0}}}{\Lambda^{\hat{0}}{}_{\hat{c}}k^{\hat{c}}}}e^{\hat{a}}_{\sigma}(\hat{\mathbf{k}},\sigma)\exp\left(i\sigma\psi(\Lambda,n^{\hat{i}})\right); \\ &k^{\hat{a}} = \left(k^{\hat{0}},\hat{\mathbf{k}}\right). \end{aligned} \tag{11}$$

Here, $M(\Lambda)$ and σ represent representation of the Lorentz transformation and helicity of a photon. Accordingly, the Wigner Rotation induces phase delay or advance of circular polarized photon states, depending on the sign of the helicity, and rotates the linear-polarization vector, $\varepsilon^{\hat{a}}_{\phi}$, by WRA in the standard frame such that[42]

$$\begin{aligned} M(\Lambda)^{\hat{a}}{}_{\hat{b}}\,\varepsilon^{\hat{b}}_{\phi} &= \left(e^{i\phi}e^{\hat{a}}_{\sigma=1} + e^{-i\phi}e^{\hat{a}}_{\sigma=-1}\right) \\ &= \left(e^{i(\phi+\psi(\Lambda,n^{\hat{i}}))}e^{\hat{a}}_{\sigma=1} + e^{-i(\phi+\psi(\Lambda,n^{\hat{i}}))}e^{\hat{a}}_{\sigma=-1}\right) \\ &= R_{\hat{z}}\left(\psi(\Lambda,n^{\hat{i}})\right)^{\hat{a}}{}_{\hat{b}}\,\varepsilon^{\hat{b}}_{\phi} = \varepsilon^{\hat{a}}_{\phi'=\phi+\psi(\Lambda,k)} \end{aligned} \tag{12}$$

where $R_{\hat{z}}(\psi)$ is the rotation about $\hat{z}$-axis by the total WRA ψ.

Chapter 3. Wigner Rotation of a photon state under the gravitational field of Earth

In this chapter, we demonstrate the existence of a non-trivial Wigner rotation experienced by photons sent non-radially from Earth ground station to a free-falling observer with non-zero angular momentum and various altitudes. To focus on the existence of a measurable WRA, we simplify the spacetime of Earth, considering only the monopole of Earth. Examining circular orbits with non-zero quantum-phase Wigner rotation components, it is found that there is a potentially measurable the Wigner rotation angle in addition to the rotation of standard fame, which agrees well with the geodetic rotation, measured by Gravity Probe B in 2011[24,29,51], and in the former case, the additional phase is dominant to the near-zero geodetic rotation. Our results show that the Wigner rotation involves a non-trivial semi-classical effect of quantum field theory on a background classical gravitational field in addition to classical geodetic precession. This finding could open up the testbed to probe gravitational effects on various quantum phenomena in a satellite by the interplay of two pillars of physics.

3.1. Earth-satellite system

Considering only the monopole of Earth, we model the spacetime around Earth with Schwarzschild spacetime where tetrad fields can be globally defined as orientation-preserved coordinate bases[38,48,52], and the (- + + +) metric signature is used. Furthermore, it is also assumed[52] that quantum field theories on spacetime admit a spinor structure[36,43,53] which will be employed for the quantum state of the photon with a given polarization.

We consider an Earth-satellite system depicted in Fig. 1. Figure 1a shows the Earth-Satellite system and corresponding coordinates. A photon is sent along its geodesic, represented by the red line, and its polarization, represented by the light-green arrows, is measured in the local frame of a satellite. The Schwarzschild metric is used to model spacetime around Earth and choose spacelike components of the tetrads so that the first, second, and third axis of the local frames become unit vectors of Schwarzschild coordinates r, θ, and φ at infinity, i.e., $\hat{e}_{\hat{a}}{}^{\mu}(\mathbf{x}_{\infty}) \equiv \hat{e}_{b}{}^{\mu}$ where $\hat{a}$ = 1, 2, and 3 correspond to $b = r$, θ, and φ, respectively. To compare the polarization measured at the surface of Earth and the satellite, the standard frame is introduced in which a wave vector of the photon is aligned to the third axis of observer's local frames (Fig.1b and 1c).

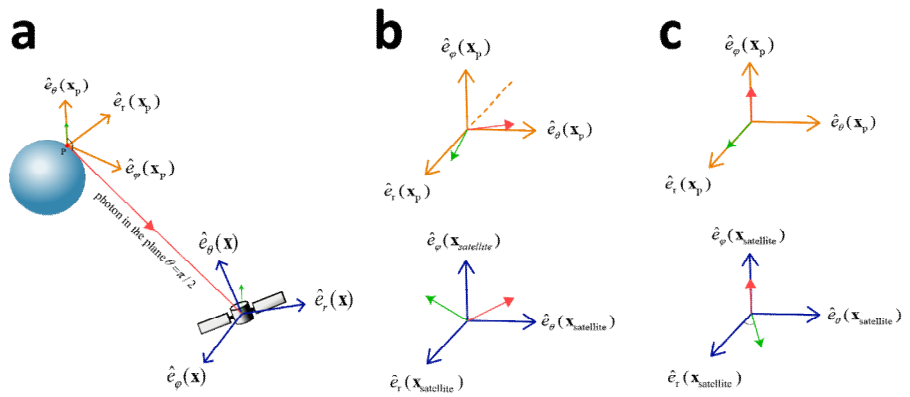

Figure 1 | Schematics of the Earth-satellite system. The Earth-Satellite system and corresponding coordinates. a a photon's geodesic and its polarizations are represented by a red line and light-green arrows, respectively. **b-c** The wave vector and polarization of the photon are measured in each local frame **(b)** and compared in the standard frame **(c)**.

We consider the following four observer trajectories: a stationary observer, a radially free-falling observer, a free-falling observer with non-zero angular momentum in a circular orbit[47] (Fig.2a). While there is another orbits with angular momentum, called spiraling orbits, we focus on the circular ones which corresponds to those of satellites. To define non-spinning local frames, we apply Fermi-walker transport and parallel transport conditions for the stationary and free-falling observers respectively. Detailed works are given in the Appendix. We note that the definition of polar coordinates induces a non-physical rotation in local frames, which must be canceled out. In other words, if the photon's geodesic is in the equatorial plane $\theta = \pi/2$ (Fig. 2b and 2c), the unit vector of the coordinate r is rotated as the coordinate φ changes. Thus, the observer is assumed to move in the plane $\hat{e}_r - \hat{e}_\theta$, i.e., the constant-$\varphi$ plane (Fig. 2b and 2c), and φ-axis is chosen as the third axis of the local frames to cancel out the polar-coordinate-induced

rotation when a wave vector is aligned to φ-axis for polarization comparison. It is worth mentioning that the Wigner rotation has a zero angle in special relativity if the direction of boost (observer) and the wave vector (photon) both lie in the $\hat{x}-\hat{z}$ plane or the $\hat{y}-\hat{z}$ plane. However, if a photon moves in the $\hat{x}-\hat{y}$ plane and an observer in the orthogonal $\hat{x}-\hat{z}$ plane, the WRA is not necessarily zero[42,50]. Correspondingly, by the equivalence principle, since our observers are assumed not to move in the plane $\hat{e}_{\hat{1}}^{\mu}(\mathbf{x})-\hat{e}_{\hat{3}}^{\mu}(\mathbf{x})$, and the photon's geodesic remains in the equatorial plane $\theta=\pi/2$ (Fig. 2b and 2c), the WRA will again be non-zero.

Timelike components of the corresponding tetrads, $\hat{e}_{\mathrm{t}}^{\mu}$, are set to the 4-velocity vector of a massive particle (e.g. satellite), moving along a geodesic corresponding to each trajectory, describing the local frame of the observer. The 4-velocity vectors of the observers and the wave vector of the photon are obtained in terms of conserved quantities defined from Killing vectors of Schwarzschild spacetime (see Appendix Eq. (5)).

For circular orbits, by applying the conditions of orthogonality and non-spinning frame, tetrads have the form

$$
\begin{aligned}
&(e_{\hat{0}})^{\mu}(\mathbf{x}) = (e_{\mathrm{t}})^{\mu}(\mathbf{x}) = (\frac{1}{\sqrt{1-\frac{3r_{\mathrm{s}}}{2r}}}, 0, \frac{1}{r}\sqrt{\frac{r_{\mathrm{s}}}{2r}}\frac{1}{\sqrt{1-\frac{3r_{\mathrm{s}}}{2r}}}, 0) \\
&(e_{\hat{1}})^{\mu}(\mathbf{x}) = (e_{\mathrm{r}})^{\mu}(\mathbf{x})(-\sqrt{\frac{r_{\mathrm{s}}}{2r}}\frac{\sin\tilde{\Theta}(r)}{\sqrt{1-\frac{3r_{\mathrm{s}}}{2r}}\sqrt{1-\frac{r_{\mathrm{s}}}{r}}}, \sqrt{1-\frac{r_{\mathrm{s}}}{r}}\cos\tilde{\Theta}(r), -\frac{1}{r}\frac{\sqrt{1-\frac{r_{\mathrm{s}}}{r}}\sin\tilde{\Theta}(r)}{\sqrt{1-\frac{3r_{\mathrm{s}}}{2r}}}, 0) \\
&(e_{\hat{2}})^{\mu}(\mathbf{x}) = (e_{\theta})^{\mu}(\mathbf{x})(\sqrt{\frac{r_{\mathrm{s}}}{2r}}\frac{\cos\tilde{\Theta}(r)}{\sqrt{1-\frac{3r_{\mathrm{s}}}{2r}}\sqrt{1-\frac{r_{\mathrm{s}}}{r}}}, \sqrt{1-\frac{r_{\mathrm{s}}}{r}}\sin\tilde{\Theta}(r), \sqrt{1-\frac{r_{\mathrm{s}}}{r}}, \frac{1}{r}\frac{\sqrt{1-\frac{r_{\mathrm{s}}}{r}}\cos\tilde{\Theta}(r)}{\sqrt{1-\frac{3r_{\mathrm{s}}}{2r}}}, 0) \\
&(e_{\hat{3}})^{\mu}(\mathbf{x}) = (e_{\varphi})^{\mu}(\mathbf{x}) = (0, 0, 0, \csc\theta / r),
\end{aligned}
\tag{13}
$$

where $\tilde{\Theta}(r) = \sqrt{1-\frac{3r_{\mathrm{s}}}{2r}}(\theta - \theta_0)$.

We set conserved energy, $\varepsilon_{\mathrm{photon}}$, of a photon to its frequency to satisfy equivalence principle, and set the energy per unit mass, $\varepsilon_{\mathrm{obs}}$, of an observer to one, in the units where $\hbar = G = c = 1$ since $\varepsilon_{\mathrm{obs}} = (1 - r_{\mathrm{s}} / r)dt / d\tau \approx 1$. We set the (non-radial) launching angle of the photon as 45° (Fig. 2b) by setting an angular momentum of a photon l_{ph} as $\frac{\omega r_{\mathrm{Earth}}}{\sqrt{2}}$ so that the radial and polar components of the wave vector have the same value on the surface of Earth, $k^{\mathrm{r}}(r_{\mathrm{Earth}}) = rk^{\varphi}(r_{\mathrm{Earth}})$. Here, ω is an angular frequency of a photon. Details of derivation are provided in the Appendix.

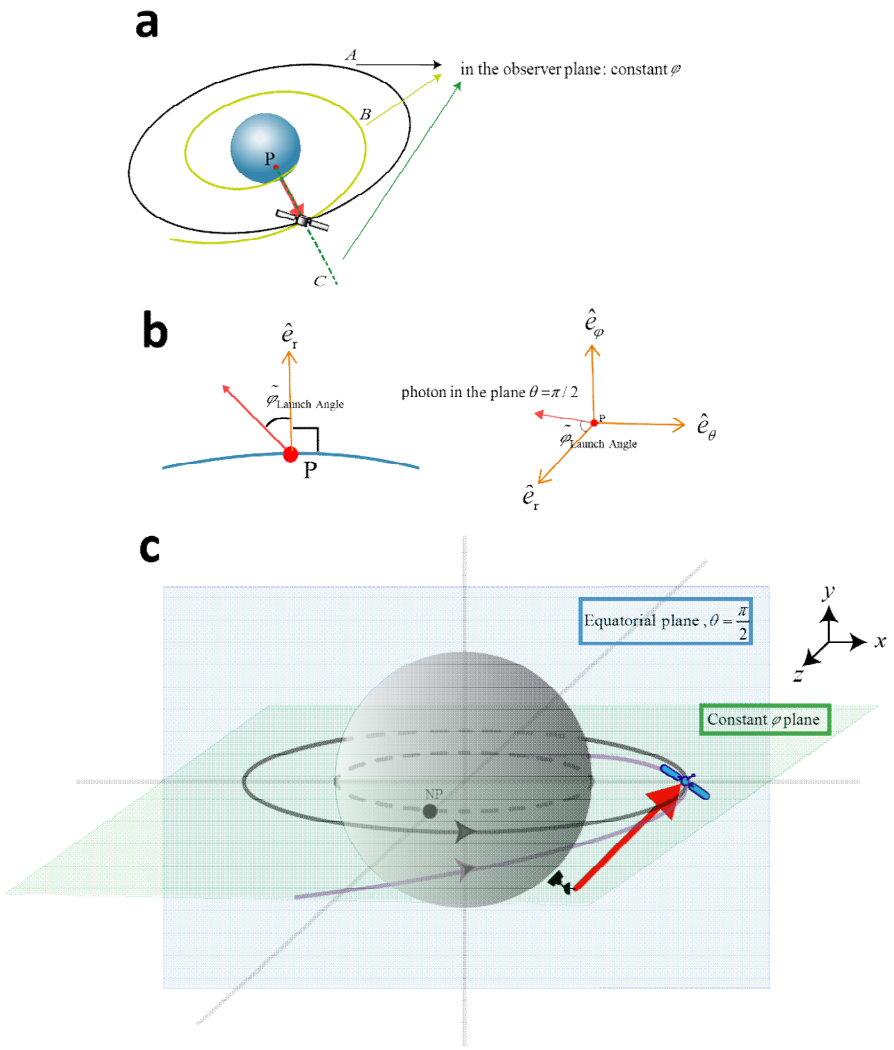

Figure 2 | Schematics of the trajectory of the observer (satellite) and photon. The geodesics of a photon traveling lies in the equatorial plane, $\theta = \pi/2$ and the observer's geodesics is lying in the constant φ-plane (the point NP on the sphere represents the North Pole). **a** A, B, and C represent the geodesics of massive free-falling observers radially, in a circular orbit, and spiraling orbit, respectively. **b-c** The non-radial launching angle of a photon from the surface of the Earth to the satellite in a Fig.2c circular (gray) and spiraling (purple) orbit in the constant-φ plane.

3.2. The Wigner rotation under the gravitational fields

Upon observation of Eqs. (9) and (10), it is noted that if every parameter is real, then the result of this equation is always real. In other words, WRA $\psi(\Lambda, n^{\hat{i}})$ must be $2m\pi$ where m is an integer. Accordingly, the first and second observer trajectories considered (stationary, radially free-falling) have zero WRAs[42] since all the parameters are real. In the opposite case where every parameter is not real, the non-zero infinitesimal Wigner rotation angle for a photon helicity state can be obtained such that

$$\begin{aligned}\tilde{\psi}_{\text{inf}} &= 2\,\text{Im}(\tilde{\alpha}) + \left[\frac{2n^{\hat{1}}}{1+n^{\hat{3}}}\text{Im}(\tilde{\beta}) + \frac{2n^{\hat{2}}}{1+n^{\hat{3}}}\text{Re}(\tilde{\beta})\right] \\ &= \lambda^{\hat{1}}{}_{\hat{2}} + \left[\frac{n^{\hat{1}}}{1+n^{\hat{3}}}\left(-\lambda^{\hat{0}}{}_{\hat{2}} + \lambda^{\hat{2}}{}_{\hat{3}}\right) + \frac{n^{\hat{2}}}{1+n^{\hat{3}}}\left(\lambda^{\hat{0}}{}_{\hat{1}} + \lambda^{\hat{3}}{}_{\hat{1}}\right)\right] \\ &\equiv \tilde{\psi}_{\text{inf}}^{\text{geodetic}} + \tilde{\psi}_{\text{inf}}^{\text{residual}}\end{aligned} \tag{14}$$

which corresponds to the last case considered, namely free-falling observers with angular momentum in a circular trajectory. Here, $\tilde{\alpha}$ and $\tilde{\beta}$ are defined as Appendix Eq. (34). We note that IWRA consists of a classical geodetic precession around the third axis, $\tilde{\psi}_{\text{inf}}^{\text{geodetic}} = 2\,\text{Im}(\tilde{\alpha})$, and a residual phase (or "residual gauge transformation") induced with the gauge-fixing for a finite irreducible unitary representation, $\tilde{\psi}_{\text{inf}}^{\text{residual}} = \frac{2n^{\hat{1}}}{1+n^{\hat{3}}}\text{Im}(\tilde{\beta}) + \frac{2n^{\hat{2}}}{1+n^{\hat{3}}}\text{Re}(\tilde{\beta})$. The total Wigner rotation angle ψ can be obtained via a time-ordered integration of IWRAs over the geodesic trajectory $x(\xi)$ of the photon such that

$$
\begin{aligned}
& e^{i\psi(\Lambda,\vec{n})} = e^{i\psi^{\text{geodetic}}(\Lambda,\vec{n})+i\psi^{\text{residual}}(\Lambda,\vec{n})} \\
& = T\exp\left[i\int \tilde{\psi}_{\text{inf}}^{\text{geodetic}}(\Lambda(x(\xi)), n^{\hat{i}}(\xi))d\xi \right] \\
& + T\exp\left[i\int \tilde{\psi}_{\text{inf}}^{\text{residual}}(\Lambda(x(\xi)), n^{\hat{i}}(\xi))d\xi \right].
\end{aligned} \tag{15}
$$

where T represents the time-ordering operator. The total geodetic-precession contribution WRA ψ^{geodetic}, and the residual phase ψ^{residual} are defined as integration of the infinitesimal WRA $\tilde{\psi}_{\text{inf}}^{\text{geodetic}}$, and $\tilde{\psi}_{\text{inf}}^{\text{residual}}$, respectively, along the photon's geodesics. The WRA for massless particles arises from a consideration of the unitary representation of the transformation of quantum single-particle states under classical Lorentz transformations, and hence manifests itself as a phase factor[35,36,42,50] depending only on direction of the photon's momentum but not its frequency. Others in the literature have ascribed the WRA to a residual gauge transformation, and the classical and quantum nature of this non-trivial phase factor remains an open question[54].

The classical geodetic contribution corresponds to the rotation around the wave vector in the standard frame, where polarization vectors are measured and compared. For the circular-orbit case, parallel transport compensates the rotation induced by spherical coordinates such that spacelike components of the tetrads are rotated by θ when an observer moves by $-r\theta$, leading to a small (almost zero, see Table 1), total classical geodetic WRA. The classical geodetic effects calculated with tetrads are compared with experimental data reported by C.W.F.Everitt et al.[30]

In Table 1, we compare the finite (i) total WRA ψ_{total}, (ii) classical geodetic contribution of the WRA $\psi_{\text{total}}^{\text{geodetic}}$, and (iii) the residual phase of the WRA $\psi_{\text{total}}^{\text{residual}}$, for circular orbits, obtained by integrating the IWRA $\tilde{\psi}_{\text{inf}}$, $\tilde{\psi}_{\text{inf}}^{\text{geodetic}} = 2\,\text{Im}(\tilde{\alpha})$, and $\tilde{\psi}_{\text{inf}}^{\text{residual}} = \frac{2n^{\hat{1}}}{1+n^{\hat{3}}}\text{Im}(\tilde{\beta}) + \frac{2n^{\hat{2}}}{1+n^{\hat{3}}}\text{Re}(\tilde{\beta})$, respectively, along the photon orbit, from the surface of Earth to the altitudes of various Earth orbits. Details of the approximation and interpolation methods employed to compute the total WRA from the IWRA, and to verify their validity are described in detail in the Appendix.

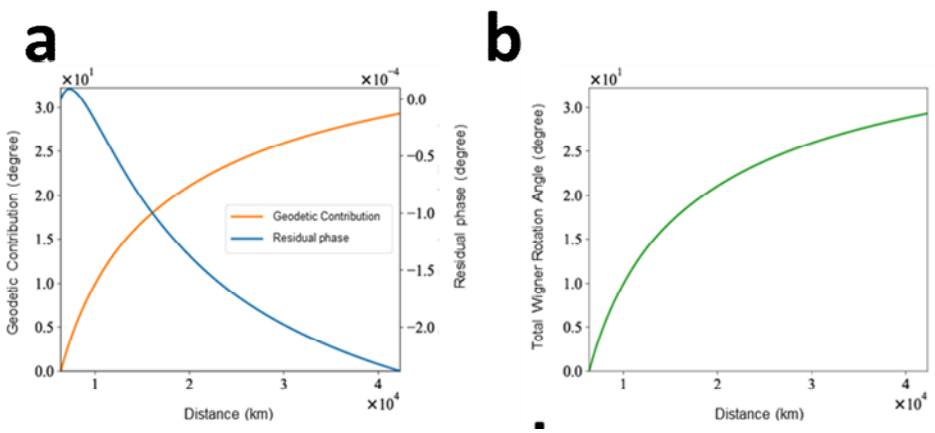

Figure 3 | WRA along distances from Earth. It is shown that the classical geodetic part in the solid orange line, the residual phase part in the solid blue line, and total WRA in green line for the circular orbit (**a**, **b**).

Table 1 shows the total ψ_{total} WRA as well as its classical geodetic $\psi_{\text{total}}^{\text{geodetic}}$ and residual $\psi_{\text{total}}^{\text{residual}}$ phases for a circular observer orbit (here envisioned as a satellite). Further details of the photon's and the observer's orbits can be found in the Supplemental Material). For the circular orbit (with the photon launched non-radially from the Earth, Fig.2C), Table 1 reveals that the

classical (general relativistic) geodetic contribution to the total WRA is effectively zero while the residual phase yields the dominant contribution in the range of $\left[2.42\times10^{-5},-6.25\times10^{-4}\right]$ degrees for radial distances ranging from near-Earth orbit (NEO, 300km) to infinity. Fig. 3a shows the classical geodetic and residual phase of the total WRA for the circular case. The classical geodetic precession (general relativistic rotation), and the residual phase are represented by the solid orange and solid blue line, respectively. The total WRA is shown in Fig. 3b.

It is also found that the residual phases have path dependence unlike the classical geodetic cases: for radially emitted photon, while the classical geodetic part of WRA does not change compared to photons with angular momentum, the residual phase WRA has different values along radial distances ranging again from NEO to infinity in the range of degrees for circular orbits (See Appendix Table 2).

Table 1. Comparison of total integrated Wigner rotation angle (WRA) , classical geodetic contribution to the WRA , and residual quantum-phase contribution to the WRA (in deg), for a satellite at various altitudes for circular orbits.

Observer in a Circular Orbit			
Altitude	**Wigner rotation angle (WRA) (Geodetic + Residual phase)** ψ_{total}	**Geodetic part of the WRA** $\psi_{\text{total}}^{\text{geodetic}}$	**Residual phase part of the WRA** $\psi_{\text{total}}^{\text{residual}}$
300km (NEO)	2.42×10^{-5}	-6.46×10^{-14}	2.42×10^{-5}
2000km (LEO)	9.64×10^{-5}	-3.03×10^{-13}	9.64×10^{-5}
20000km (MEO)	-8.78×10^{-7}	-7.02×10^{-13}	-8.78×10^{-7}
36000km (GEO)	-9.93×10^{-5}	-7.61×10^{-13}	-9.93×10^{-5}
$\mathbf{1.6\times10^{11}}$ **km** $(r=\infty)$	-6.25×10^{-4}	-8.02×10^{-13}	-6.25×10^{-4}

NEO, LEO, MEO and GEO = Near-, Low-, Medium- and Geosynchronous Earth Orbit.

Chapter 4. Dependence of angular momentums of a gravitating object and photon trajectories on Wigner rotation angles

Here, we investigate the effects on WRAs from the spinning angular momentum of gravitating object (J) axial angular momentums of photon (l_{photon}) by introducing Kerr spacetime and calculating WRAs along representative photon trajectories on the equatorial plane with different positive and negative angular momentums l_{photon} for two types of circular orbits, equatorial and polar orbits. It is demonstrated that WRAs depend on the two angular momentums, J and l_{photon}, in general by calculating WRAs for observers' frames on a thin accretion disk of a supermassive blackhole, for example, M87 with and without the spinning angular momentum J for various photon angular momentums l_{photon}. For Earth, while its small spinning angular momentum J does not add any additional phase to the WRAs up to order of 10^{-8} as assumed in many previous works[45,46] and angular momentum of photon geodesics l_{photon} changes only a minute amount of geodetic precession contribution (10^{-8}~10^{-14}) for observers' frames whose quantization axis are orthogonal to the equatorial plane, different sign of l_{photon} leads to measurable differences of residual phases in WRA for observers in the frame where the quantization axis and photons lie on the same plane. Utilizing the dependence of WRA on sign of l_{photon}, we

introduce an ‘astronomical’ Mach-Zehnder interferometer near Earth with an indistinguishable two-photon input state travelling along one of arms in combination with HOM effect; the two photon states simultaneously entering into the first beam splitter, one in each port, becomes a superposition of two-photon states emitting into each arm, as known as HOM effect. Along one of the arms, the photon state is sent to the second beam splitter in the satellites on a polar orbit after which the coincidence rates are measured. The relative WRA difference between two photon states in one of two arms variates the coincidence rates. This finding is distinguished from the features of classical interferometry since it stems from the pure quantum interferometry characteristics, HOM effect. We believe these results could provide a potential testbed of the interplay of general relativity and quantum theory.

4.1. Dependence of WRAs on angular momentums of open photon trajectories

First, we investigate the effects on WRA by angular momentums of photon l_{photon}, whose sign is intrinsically related to time reversal symmetry, along open trajectories from ground station to satellites with various ratios of azimuthal components rk^{ϕ} of the photon 4-velocity to radial one k^{r}; for a certain ratio (rk^{ϕ}/k^{r}) at a ground station, the angular momentum of photon has a unique solution whose sign follows that of ratio — l_{photon}^{+} and l_{photon}^{-} for positive and negative ratios, respectively. The Kerr metric is applied to model spacetime of Earth with spin angular momentum ($\frac{J}{Mc} = a \cong 3.9\ \text{m}$), which is given by[55]

$$\begin{aligned} ds^2 = &-\left(1-\frac{r_s r}{\Sigma}\right)c^2dt^2+\frac{\Sigma}{\Delta}dr^2+\Sigma d\theta^2 \\ &+\left(r^2+a^2+\frac{r_s r a^2}{\Sigma}\sin^2\theta\right)\sin^2\theta d\phi^2-\frac{2r_s r a\sin^2\theta}{\Sigma}cdtd\phi \end{aligned}, \quad (16)$$

where $\Sigma \equiv r^2 + a^2\cos^2\theta$, $\Delta \equiv r^2 - r_s r + a^2$, and $r_s \equiv 2GM/c^2$ is the Schwarzschild radius. $J \equiv aMc$ and M are angular momentum and the mass of the gravitating object, respectively. Throughout this paper, the (– + + +) metric signature is used and a photon field on a curved spacetime is assumed to have a spinor structure[36,43,53]. Considering that the residual term ψ^{residual} in the WRA has greater values than the geodetic-precession contribution ψ^{geodetic} for observers on circular orbits which corresponds to

satellites[45] and only the residual phase contributes to the time reversal symmetry breakdown, in this paper we focus on the case of two kinds of circular orbits, equatorial and polar orbits, represented by yellow and light blue lines respectively in Fig.4a. To describe local inertial frames of satellites, we obtain co-moving and non-spinning tetrads from Marck's ones[56]. Then, the quantization axis, the local third axis in the standard frame depicted in Fig 4b and 4c, is aligned to axis of the geodetic precession (two-order larger than the frame-dragging effect) so that its contribution to WRAs can easily be separated from momentum-dependent residual phases. It is worth mentioning that, for equatorial orbits, unphysical rotation (about θ-axis) induced by definition of radial and azimuthal coordinates is not involved in WRAs owing to the parallel-transport conditions of tetrads along the azimuthal direction. In contrast, for polar orbits, axis of the unphysical rotation is not aligned with those of satellite orbits and thus the parallel-transport conditions do not exclude the unphysical rotation. For this, by setting the axis of geodetic precession (ϕ-axis for the polar orbits) to be the local third axis, the unphysical rotation can be canceled out while aligning wave vector to the local third axis to build standard frame[52].

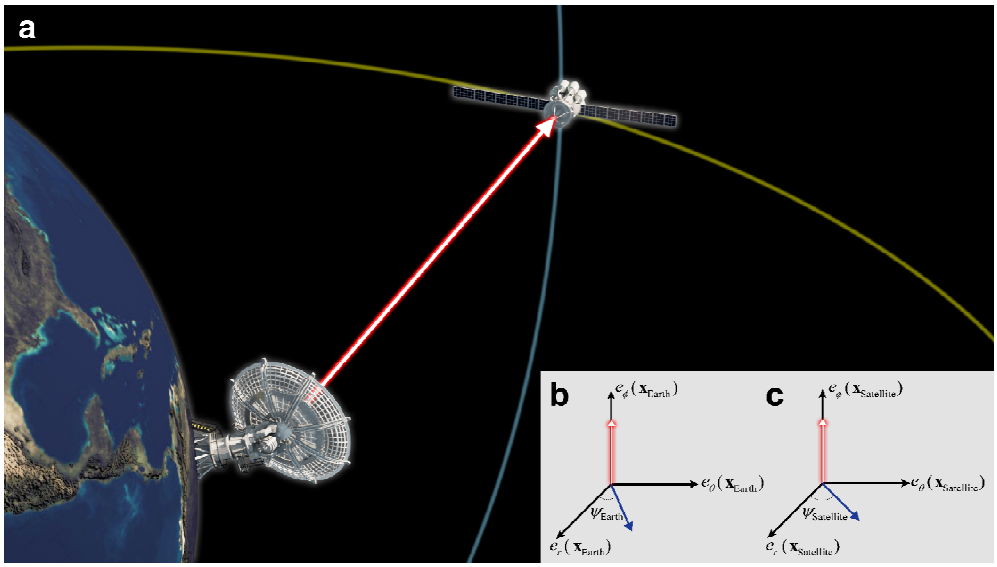

Figure 4 | Schematics of the Earth-satellite system. a a photon is sent along its geodesic to satellites on equatorial and polar orbits (yellow and light blue lines, respectively). **b-c** The wave vector (red arrows) and polarization (blue arrows) of the photon are measured in the standard frame where wave vector is aligned along the local third axis. Since there is no rest-frame for massless particles, standard frame is introduced for quantization of photon eigen-helicity states. Gravitation and satellite's 4-velocity lead to variation of polarization angle between frames on the surface of Earth (**b**) and in the satellites (**c**).

In the frame of both observer's equatorial and polar orbits near Earth, with negligible geodetic precession contributions (10^{-8}~10^{-14}), the residual phases have orders of 10^{-5} for the photon trajectory with $rk^{\phi}/k^{r}=1$ at the ground station, showing good agreement with the previous report (see Table2 and Table3). For equatorial plane, time reversal symmetry breakdown is relatively small as the quantization axis is orthogonal to the equatorial plane on which a photon moves, i.e., $\hat{n^3}$ is zero. In general, it is confirmed that signs of the photon angular momentum l_{photon} and spinning angular momentum J variate WRAs by numerical calculation for observers on equatorial orbits of a supermassive black hole, M87, while not resulting in differences up to the 3~4 significant digits near Earth along radial distances

ranging from surface of Earth to geosynchronous orbit (GEO, 30000km) as shown in Fig. 5. Figs. 5a-c show the WRAs, geodetic-contribution, and residual phases and in their insets the corresponding ΔWRAs (WRA in Kerr spacetime – WRA in Schwarzschild spacetime) for the photon emitting from $r = 4.5r_s$ with different photon angular momentum l_{photon}. Fig.5d and 5e show the local Lorentz transformation $\lambda^{\hat{3}}{}_{\hat{1}} + \lambda^{\hat{0}}{}_{\hat{1}}$ and momentum-dependent term $\frac{n^{\hat{2}}}{1+n^{\hat{3}}}\left(=n^{\hat{2}}\right)$ as representatives for the equatorial orbits near the black hole and Earth, respectively. Unlike the case of the supermassive black hole, only the signs of two terms for equatorial orbits of Earth are flipped depending on that of $l_{\text{photon}}l_{\text{photon}}$ which accordingly does not contribute to the residual phase $\psi^{\text{residual}}(\cong \psi)$ as shown in Fig. 5f.

For polar orbits, it is found that WRAs depend on the angular momentum of photon trajectory l_{photon} near Earth as well. In this case, the sign of $n^{\hat{3}}$ depends on that of photon angular momentum l_{photon} and thus leads to different order of the representative of momentum-dependent terms, $\frac{n^{\hat{2}}}{1+n^{\hat{3}}}\left(\lambda^{\hat{0}}{}_{\hat{1}} + \lambda^{\hat{3}}{}_{\hat{1}}\right)$, and naturally total WRAs ψ. In Fig. 6, WRAs, the corresponding $\frac{n^{\hat{2}}}{1+n^{\hat{3}}}\left(\lambda^{\hat{0}}{}_{\hat{1}} + \lambda^{\hat{3}}{}_{\hat{1}}\right)$, and $n^{\hat{3}}$ for the polar orbits near Earth are shown for various $l_{\text{photon}}{}^{+}$ and $l_{\text{photon}}{}^{-}$ represented with blue and green lines, respectively. It is noted that setting the local third axis to be the ϕ-axis in the

case of polar orbits leads to quite a small (~10^{-5}) but non-zero $n^{\hat{2}}$ as shown in the inset of Fig.6b. This non-trivial $n^{\hat{2}}$ values come from a special relativistic term, the product of time-component of tetrads $e_0^{\ \hat{2}}$ and photon frequency k^t. Thus, the residual phases ψ^{residual} are naturally coupled with the azimuthal component of photon momentum k^ϕ in the standard frame.

Table 2. Comparison of Wigner rotation angle (WRA) ψ, geodetic contribution ψ^{geodetic}, and residual phase ψ^{residual} (in deg), in the local frames of observers are on ***equatorial orbits*** of Earth at various altitudes with positive or negative angular momentum of photon trajectory whose rk^ϕ/k^r=1 at the ground station: (top) $l_{\text{photon}}^{\ +}$ and (bottom) $l_{\text{photon}}^{\ -}$.

Positive angular momentum of photon trajectory $l_{\text{photon}}^{\ +}$			
Altitude	Wigner rotation angle (geodetic + residual contribution) ψ_{total}	geodetic contribution to the WRA $\psi_{\text{total}}^{\text{geodetic}}$	Residual contribution of the WRA $\psi_{\text{total}}^{\text{residual}}$
300km	2.06×10^{-5}	1.67×10^{-9}	2.06×10^{-5}
2000km	4.26×10^{-5}	7.47×10^{-9}	4.26×10^{-5}
20000km	-3.36×10^{-4}	1.53×10^{-8}	-3.36×10^{-4}
36000km	-4.85×10^{-4}	1.59×10^{-8}	-4.85×10^{-4}
Negative angular momentum of photon trajectory $l_{\text{photon}}^{\ -}$			
300km	2.06×10^{-5}	1.67×10^{-9}	2.06×10^{-5}
2000km	4.26×10^{-5}	7.47×10^{-9}	4.26×10^{-5}
20000km	-3.36×10^{-4}	1.53×10^{-8}	-3.36×10^{-4}
36000km	-4.85×10^{-4}	1.59×10^{-8}	-4.85×10^{-4}

Table 3. Comparison of Wigner rotation angle (WRA) ψ_{total}, geodetic contribution $\psi_{\text{total}}^{\text{geodetic}}$, and residual phase $\psi_{\text{total}}^{\text{residual}}$ (in deg), in the local frames of observers are on ***polar orbits*** of Earth at various altitudes with positive or negative angular momentum of photon trajectory whose rk^{ϕ}/k^{r}=1 at the ground station: (top) l_{photon}^{+} and (bottom) l_{photon}^{-}.

Positive angular momentum of photon trajectory l_{photon}^{+}			
Altitude	Wigner rotation angle (geodetic + residual contribution) ψ_{total}	geodetic contribution to the WRA $\psi_{\text{total}}^{\text{geodetic}}$	Residual contribution of the WRA $\psi_{\text{total}}^{\text{residual}}$
300km	2.42×10^{-5}	6.45×10^{-14}	2.42×10^{-5}
2000km	9.63×10^{-5}	3.02×10^{-13}	9.63×10^{-5}
20000km	-7.04×10^{-7}	7.17×10^{-13}	-7.04×10^{-7}
36000km	-1.00×10^{-4}	7.59×10^{-13}	-1.00×10^{-4}
Negative angular momentum of photon trajectory l_{photon}^{-}			
300km	-2.93×10^{-4}	-6.45×10^{-14}	-2.93×10^{-4}
2000km	-1.24×10^{-3}	-3.02×10^{-13}	-1.24×10^{-3}
20000km	-2.76×10^{-3}	-7.17×10^{-13}	-2.76×10^{-3}
36000km	-2.99×10^{-3}	-7.59×10^{-13}	-2.99×10^{-3}

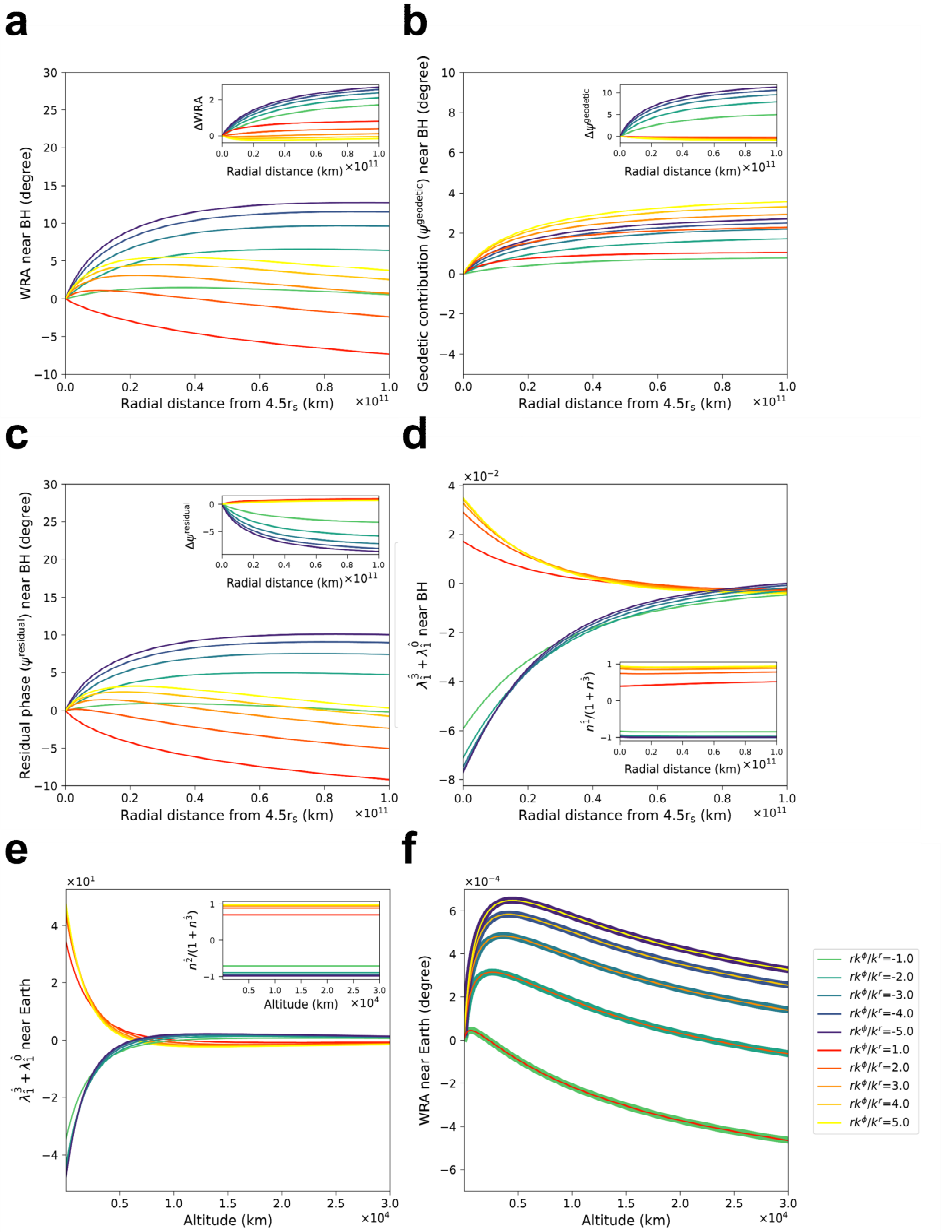

Figure 5 | WRAs for equatorial orbits. a-c WRA ψ **(a),** the geodetic contribution ψ^{geodetic} **(b)**, and residual phase ψ^{residual} **(c)** measured by observer on equatorial orbits of a supermassive blackhole M87, whose differences induced by spinning angular momentum J of the gravitating object are shown in the inset of each figure. **d-e** a representative term of the infinitesimal boost and rotation near the blackhole **(d)** and Earth **(e).** The corresponding momentum dependence term $\left(n^{\hat{2}}/\left(1+n^{\hat{3}}\right)\right)$ are in insets **WRA** of equatorial orbits of Earth**(f)**.

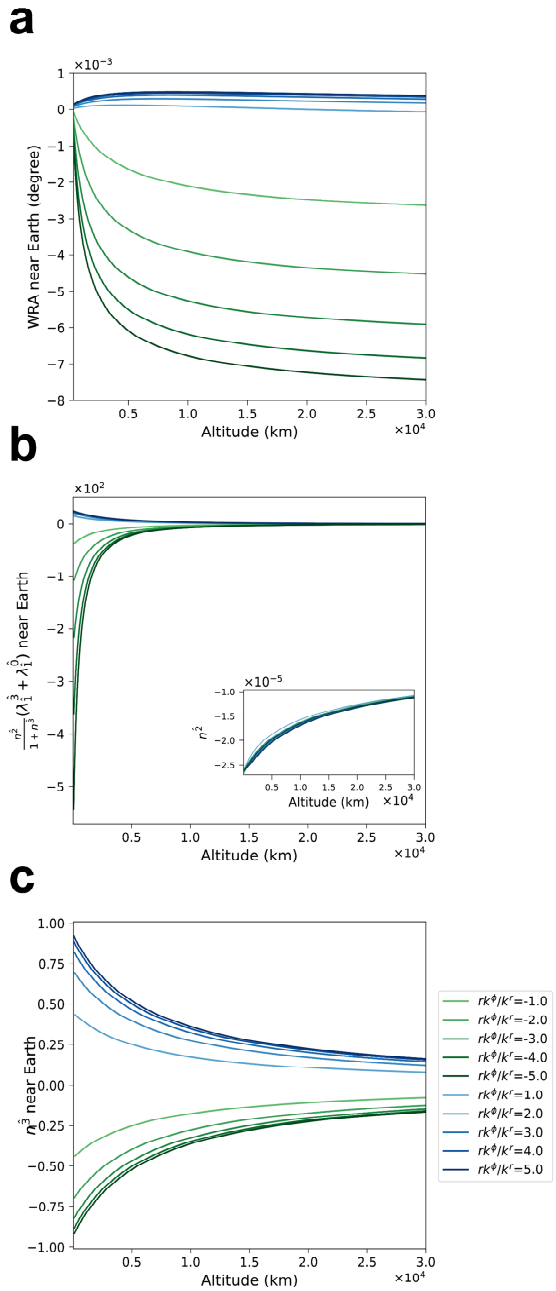

Figure 6 | WRAs, a representative of momentum dependent terms $\left(n^{\hat{2}}/\left(1+n^{\hat{3}}\right)\right)\left(\lambda^{\hat{0}}{}_{\hat{1}}+\lambda^{\hat{3}}{}_{\hat{1}}\right)$, and $n^{\hat{3}}$ for polar orbits of Earth. a WRAs measured by observer on polar orbits near Earth. **b-c** the corresponding $\left(n^{\hat{2}}/\left(1+n^{\hat{3}}\right)\right)\left(\lambda^{\hat{0}}{}_{\hat{1}}+\lambda^{\hat{3}}{}_{\hat{1}}\right)$ **(b)**, and $n^{\hat{3}}$ **(c)**.

4.2. Astronomical Interferometer

To study the interplay between WRAs and quantum interference by taking advantage of the dependence of WRA on photon angular momentum l_{photon} in local frames on polar orbits, we consider an astronomical Mach-Zehnder interferometry consisting of satellites on polar orbits as depicted in Fig. 7; two-indistinguishable circular-polarized photon state $\frac{1}{\sqrt{2}}\left(|2,0\rangle_{a_{\text{I}},b_{\text{I}}} - |0,2\rangle_{a_{\text{I}},b_{\text{I}}}\right)$ are prepared via HOM effects with the first 50:50 beam splitter in Alice's satellite on the LEO orbits (altitude, 300km). Then, photons from port a_{I} and b_{I} with a $\pi/2$ phase shifter (PS) as depicted in Fig.4b are sent to David along $\gamma 1$ and $\gamma 2$ with two different photon angular momentums l_{photon}^{+} and l_{photon}^{-}, respectively. The final output state passing through the second beam splitter in David's frame (Fig. 7c) becomes

$$-i\left(\frac{1+ie^{\sigma i\Delta\psi}}{2\sqrt{2}}\left(|2,0\rangle_{a_{\text{II}},b_{\text{II}}} + |0,2\rangle_{a_{\text{II}},b_{\text{II}}}\right) + \frac{-1+ie^{\sigma i\Delta\psi}}{2}|1,1\rangle_{a_{\text{II}},b_{\text{II}}}\right) \qquad (17)$$

with the relative phase differences $\Delta\psi = \left(\int_{\gamma_1}\tilde{\psi}_{\text{inf}}d\xi - \int_{\gamma_2}\tilde{\psi}_{\text{inf}}d\xi\right)$ and the coincidence rate (1-sin($\Delta\psi$))/2. Fig.7d shows the differences of the coincidence rates ($\approx \Delta\psi/2$) induced by path-dependence of WRAs for different altitudes of David. With the negligible geodetic-precession contribution ψ^{geodetic}, the residual phase ψ^{residual} leads to measurable differences in coincidence rates, which corresponds to 10^8 counts/ms photon

count rates when a photon pulse of 1mW power arrives at David's frame. Moreover, it is worth mentioning this interplay between the coincidence rates and relative WRAs in the quantum interferometer are distinguished from that of classical interferometers as discussed by Simanraj Sadana et al[57]. Since HOM effect doesn't occur at the first beam splitter for classical light, interference of photon states from each arm doesn't occur at the second beam splitter and thus changes of coincidence rates either.

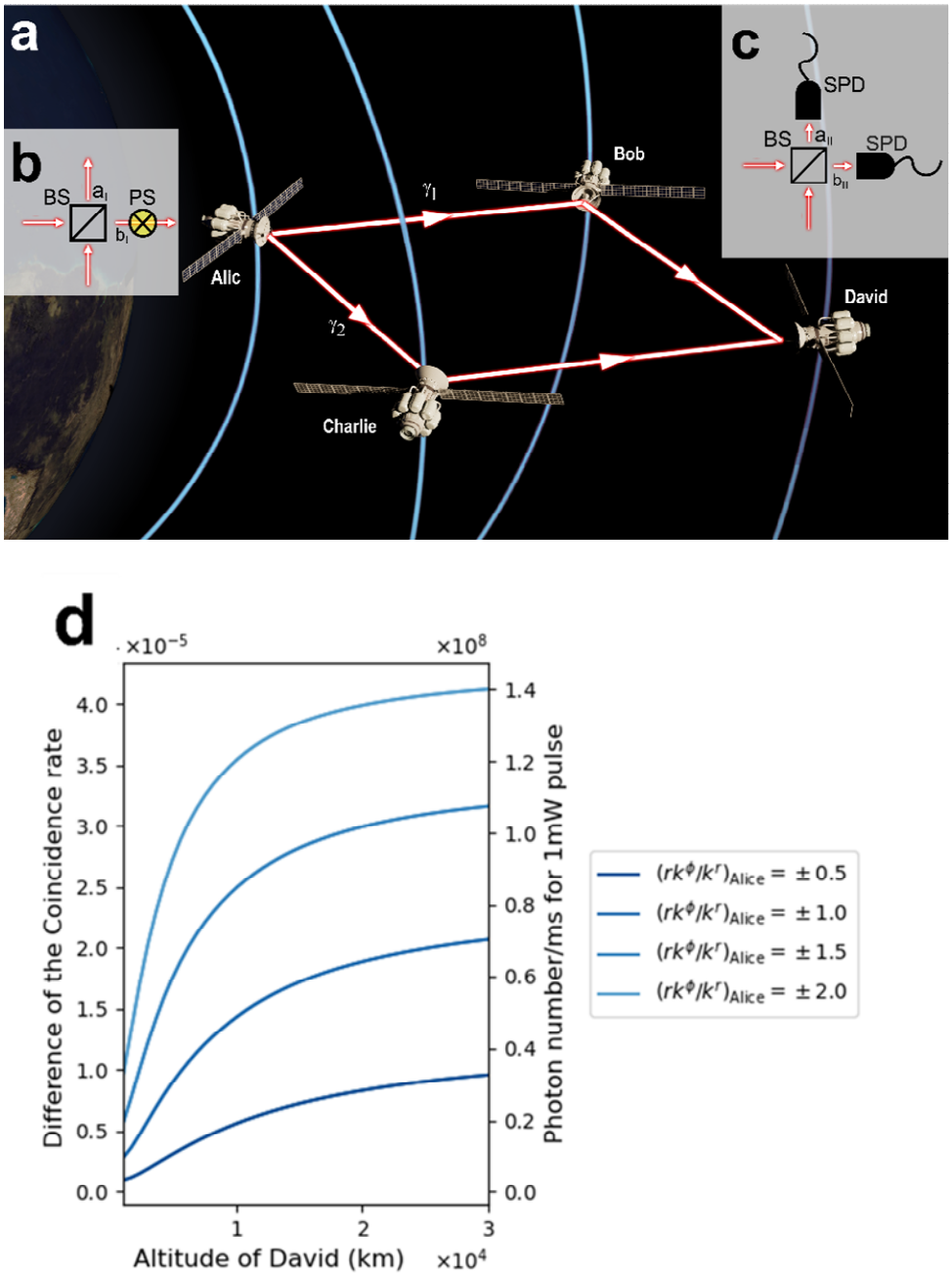

Figure 7 | **a** Astronomical Mach-Zehnder Interferometer. **b** Hong-Ou-Mandel effects occur in Alice's frame. **c** Photons sent out from Alice to Bob and Charlie are reflected to David and then passed through the BS (Beam-Splitter). **d** the variation of coincidence rates induced by WRAs and the corresponding photon count rates for 1mW-power photon pulse with σ=1**.**

Chapter 5. Conclusion

Here, the Wigner rotation of a photon state is investigated in Schwarzschild and Kerr spacetimes to study a rotation of its polarization, considering only the monopole of Earth. While the quadrupole of Earth could induce non-negligible effect on WRA[58] and ionosphere and vanAllen belts could rotate the polarization vector of a photon, we focus on showing that there is an additional and measurable WRA in addition to the geodetic precession. We calculate the wave vector of the photon to obtain infinitesimal local Lorentz transformations for the four cases of a stationary observer, a free-falling observer with zero angular momentum, and free-falling observers with angular momentum in a circular orbit. For the first two cases, the calculated Wigner rotation angles (WRA) are zero. We calculate the non-zero WRA for the last two cases in two different ways: (i) by using physically meaningful approximations and (ii) by an interpolation method (see Appendix) for verification of our results since the differential equation for the photon's trajectory is challenging to solve analytically, and the tetrads for circular orbits have a complex a form that inhibits easy physical interpretations. It is found that two different approaches give the same results up to 7 significant figures. The circular orbit results in a WRA whose classical geodetic contribution is effectively zero for all practical measurements, yet whose contribution is 2.42×10^{-5} degrees at NEO, and -6.25×10^{-4} degrees at infinity. Their effect (sine squared value) on the quantum bit error rate

(QBER) is effectively zero.

It is also interesting to compare these results with the works by Connors et al.[59], who estimated the polarization rotation angle of 82° at infinity from the X-rays near a black hole in Cygnus X-1 by using the general relativistic calculations. Our approach can also be applied to the astronomical measurement of the rotation of the photon polarization from the black holes such as recently observed M87. In addition, if one is able to measure the polarization rotation of a photon passing both far from (predominantly classical geodetic contribution to the WRA) and close by (classical geodetic + residual phase) a massive gravitating object, and then take the difference between the two rotation angles, one would have a measure of the residual quantum-phase contribution to the WRA.

Also, we study the effects of WRAs on the coincidence rates of an astronomical Mach-Zehnder interferometer. After passing through the first beam splitter, two indistinguishable photon states evolve with different WRAs along one of two arms of the interferometer, which leads to interference in the second beam splitter and thus variations of coincidence rates. It is found that, for the polar orbits where the quantization axes are not orthogonal to the wave vectors of photons, the residual phases ψ^{residual} depends on the sign of azimuthal- component wave vector k^{ϕ} as opposed to the case of equatorial orbits. Thus, the relative phase differences of them $\Delta\psi^{\text{residual}}$ vary the coincindence rates from the second beam splitter. It is contro

versial if the momentum-dependent residual phase ψ^{residual} is classical or qu antum effect. It is stressed that measurable order of the residual phase in W RA ψ^{residual} can be mingled with the pure quantum optical feature, HOM eff ect and the coincidence rates in an astronomical Mach-Zehnder interferomet ry owing to the time reversal symmetry breakdown and special relativistic c oupling between azimuthal component of photon velocity k^{ϕ} and WRA. While there has been much renewed interest in the effects of the gravitational field on quantum systems, especially in relation to the effect of accelerated motion and horizons on quantum entanglement[60-62] inspired by the seminal work of Hawking[63] and Unruh[64], less work has been performed on an experimental assessment of the regime in which quantum systems evolve on classical curved spacetime. The proposed model in this dissertation could provide a testbed for probing the gravitational effects on quantum systems.

Appendix

A1. Massive and Massless particles' trajectory in Schwarzschild metric

In general relativity, it is well known that the Lagrangian, L, can be chosen in the form

$$\frac{1}{2}\left(\frac{ds}{d\xi}\right)^2 \tag{A1}$$

with the line element for the Schwarzschild metric, which is defined as follows

$$ds^2 = -\left(1-\frac{r_s}{r}\right)^2 dt^2 + \left(1-\frac{r_s}{r}\right)^{-1} dr^2 + r^2 d\theta^2 + r^2 \sin^2\theta d\phi^2. \tag{A2}$$

Here, ξ represents proper time and an affine parameter for massive and massless particles, respectively. If the Lagrangian has no dependence on specific coordinates, x^μ, the equations of motion imply the conservation of corresponding quantities. In other words, from the equations of motion,

$$\frac{d}{d\xi}\left(\frac{\partial L}{\partial(\mathrm{d}x^\mu/\mathrm{d}\xi)}\right) = \frac{dL}{dx^\mu} = 0, \tag{A3}$$

the following identities hold:

$$\frac{\partial L}{\partial(\mathrm{d}x^\mu/\mathrm{d}\xi)} = g_{\mu\beta}\frac{dx^\beta}{d\xi} = g_{a\beta}\delta_\mu{}^\alpha \frac{dx^\beta}{d\xi} = g_{\alpha\beta}\frac{\partial x^\alpha}{\partial x^\mu}\frac{dx^\beta}{d\xi} = \frac{\partial}{\partial x^\mu}\cdot\frac{dx}{d\xi} = const \tag{A4}$$

.

Since time t and azimuthal angle ϕ are cyclic coordinates in Schwarzschild spacetime, two quantities e and l are conserved, defined by

$$e \equiv -\frac{\partial}{\partial t}\cdot\frac{d\mathbf{x}}{d\xi} = \left(1-\frac{r_s}{r}\right)\frac{dt}{d\xi},\ l \equiv -\frac{\partial}{\partial \phi}\cdot\frac{d\mathbf{x}}{d\xi} = r^2\sin^2\theta\frac{d\phi}{d\xi}. \quad \text{(A5)}$$

For an observer, massive particle, e_{obs} and l_{obs} are called energy per unit rest mass at very large r and angular momentum per unit rest mass at very low velocities, respectively[1]. The normalization condition of 4-velocity vectors can be rewritten as

$$-\frac{{e_{obs}}^2}{\left(1-\frac{r_s}{r}\right)}+\frac{1}{\left(1-\frac{r_s}{r}\right)}\left(\frac{dr}{d\xi}\right)^2+\frac{l_{obs}}{r^2}=-1. \quad \text{(A6)}$$

Correspondingly, the radial component of (outgoing) 4-velocity vectors have the form:

$$\frac{dr}{d\xi}=\sqrt{{e_{ph}}^2-\left(1+\frac{l_{ph}}{r^2}\right)\left(1-\frac{r_s}{r}\right)}. \quad \text{(A7)}$$

For a photon, a massless particle, e_{ph} and l_{ph} represent energy and angular momentum at infinity, respectively[47]. With these quantities, photon's null world line can be described as

$$-\frac{{e_{ph}}^2}{\left(1-\frac{r_s}{r}\right)}+\frac{1}{\left(1-\frac{r_s}{r}\right)}\left(\frac{dr}{d\xi}\right)^2+\frac{l_{ph}}{r^2}=0. \quad \text{(A8)}$$

Likewise, the radial component of the wave vector has the form:

$$\frac{dr}{d\xi}=\sqrt{{e_{ph}}^2-\frac{l_{ph}}{r^2}\left(1-\frac{r_s}{r}\right)}=e_{ph}\sqrt{1-\frac{{b_{ph}}^2}{r^2}\left(1-\frac{r_s}{r}\right)} \quad \text{(A9)}$$

Thus, the explicit forms of a wave vector and its dual vector become

$$k^{\mu}(x)=\left(\frac{e_{ph}}{1-\frac{r_s}{r}},e_{ph}\sqrt{1-\frac{{b_{ph}}^2}{r^2}\left(1-\frac{r_s}{r}\right)},\frac{e_{ph}b_{ph}}{r^2},0\right), \tag{A10}$$

and

$$k_{\mu}(x)=\left(-e_{ph},\frac{e_{ph}}{1-\frac{r_s}{r}}\sqrt{1-\frac{{b_{ph}}^2}{r^2}\left(1-\frac{r_s}{r}\right)},e_{ph}b_{ph},0\right) \tag{A11}$$

By Equivalence principle, wave (co)vectors in the local inertial frame, defined with radially free-falling tetrads, should have the same form with the wave (co)vectors in flat spacetime, as follows:

$$k_{\hat{a}}(x)=\left(-\omega,k_{\hat{1}},k_{\hat{2}},k_{\hat{3}}\right),\quad \text{where } \omega=\sqrt{\left(k_{\hat{1}}\right)^2+\left(k_{\hat{2}}\right)^2+\left(k_{\hat{3}}\right)^2}\,. \tag{A12}$$

In other words, the inner product of wave covector k_{μ} and the timelike tetrad $e_{\hat{0}}{}^{\mu}$ of Eq. S57 should be the same as the angular frequency of a photon observed in flat spacetime, i.e.,

$$\begin{aligned} k_{\hat{0}}(x) &\cong -\frac{e_{ph}}{1-\frac{r_s}{r}}\left(1+\sqrt{\frac{r_s}{r}}\sqrt{1-\frac{{b_{ph}}^2}{r^2}\left(1-\frac{r_s}{r}\right)}\right) \\ &\cong -e_{ph}\left(1+\frac{r_s}{r}+\sqrt{\frac{r_s}{r}}\sqrt{1-\frac{{b_{ph}}^2}{r^2}\left(1-\frac{r_s}{r}\right)}\right)\cong -\omega. \end{aligned} \tag{A13}$$

Therefore, we can conclude that the photon's energy is the same as the frequency of the photon, measured at the $r=\infty$. To get the explicit expression of photon's trajectory, the following differential equation needs solving:

$$k^r = \frac{dr}{d\xi} = \sqrt{\omega^2 - \frac{{l_{photon}}^2}{r(\xi)^2} + \frac{{l_{photon}}^2}{r(\xi)^2}\frac{r_s}{r(\xi)}}\,. \qquad \text{(A14)}$$

Since Eq. A14 is challenging to be solved analytically, we ignore the last term $\frac{{l_{photon}}^2}{r(\xi)^2}\frac{r_s}{r(\xi)}$ by taking advantage of the fact that the order of $\frac{r_s}{r}$ is 10^{-9} near the surface of Earth.

A2. Massive and Massless particles' trajectory in Kerr metric

Geodesics of a particle in Kerr spacetime is described by

$$\begin{pmatrix} \frac{dt}{d\xi} \\ \frac{dr}{d\xi} \\ \frac{d\theta}{d\xi} \\ \frac{d\phi}{d\xi} \end{pmatrix} = \begin{pmatrix} \frac{1}{\Delta\Sigma}\left(E\left[\left(r^2+a^2\right)^2 - \Delta a^2 \sin^2\theta\right] - 2Mra\Phi\right) \\ \pm\frac{1}{\Sigma}\sqrt{\left(E\left(r^2+a^2\right)^2 - a\Phi\right)^2 - \Delta\left(K+\delta_1 r^2\right)} \\ \pm\frac{1}{\Sigma}\sqrt{K - \delta_1 a^2\cos^2\theta - \left(aE\sin\theta - \Phi/\sin\theta\right)^2} \\ \frac{1}{\Delta\Sigma}\left(2MraE + \left(\Sigma - 2Mr\right)\Phi/\sin^2\theta\right) \end{pmatrix}. \qquad \text{(A15)}$$

Here, $K \equiv Q+(\Phi-aE)^2$. The paremeters (ξ , δ_1) are (affine parameter, 0) or (proper time , 1) for null or time-like geodesics, respectively. E, Φ, and Q are the energy, axial angular momentum, and Carter constant of a particle. Φ of observers and photons are rewritten as l_{obs} and l_{photon} in this paper.

We obtained tetrads for this work by transforming Carter's sysmmetric tetrads used in Marck's tetrads $\left\{\boldsymbol{\lambda}_{\hat{i}} = \left(\lambda_{\hat{i}}{}^{t}, \lambda_{\hat{i}}{}^{r}, \lambda_{\hat{i}}{}^{\theta}, \lambda_{\hat{i}}{}^{\phi}\right) | i = 0,1,2,3\right\}$ back to BL-coordinate bases. Marck's tetrads and the transformation are as follows:

$$\begin{pmatrix}\lambda_{\hat{0}}\\ \lambda_{\hat{1}}\\ \lambda_{\hat{2}}\\ \lambda_{\hat{3}}\end{pmatrix}=\begin{pmatrix}1 & 0 & 0 & 0\\ 0 & \cos\Psi & 0 & -\sin\Psi\\ 0 & 0 & 1 & 0\\ 0 & \sin\Psi & 0 & \cos\psi\end{pmatrix} \tag{A16}$$
$$\times\begin{pmatrix}\sqrt{\Delta/\Sigma}\left(e_{\hat{0}}{}^{t}-a\sin^2\theta e_{\hat{0}}{}^{\phi}\right) & \sqrt{\Sigma/\Delta}e_{\hat{0}}{}^{r} & \sqrt{\Sigma}e_{\hat{0}}{}^{\theta} & \left(ae_{\hat{0}}{}^{t}-\left(r^2+a^2\right)e_{\hat{0}}{}^{\phi}\right)\sin\theta e_{\hat{0}}{}^{t}/\sqrt{\Sigma}\\ \alpha\sqrt{\Sigma/K\Delta}re_{\hat{0}}{}^{r} & \alpha\sqrt{1/K\Sigma\Delta}rC & \beta\sqrt{1/K\Sigma}a\cos\theta D & -\beta\sqrt{\Sigma/K}a\cos\theta e_{\hat{0}}{}^{\theta}\\ \sqrt{\Sigma/K\Delta}a\cos\theta e_{\hat{0}}{}^{r} & \sqrt{1/K\Sigma\Delta}a\cos\theta C & -\sqrt{1/K\Sigma}rD & \sqrt{\Sigma/K}re_{\hat{0}}{}^{\theta}\\ \alpha\sqrt{1/\Sigma\Delta}C & \sqrt{1/K\Sigma\Delta}a\cos\theta C & \beta\sqrt{\Sigma}e_{\hat{0}}{}^{\theta} & \beta\sqrt{1/\Sigma}D\end{pmatrix}$$

with $C=E\left(r^2+a^2\right)-a\Phi$ and $D=aE\sin\theta-\Phi/\sin\theta$

$$\begin{pmatrix}e_{\hat{i}}{}^{t}\\ e_{\hat{i}}{}^{r}\\ e_{\hat{i}}{}^{\theta}\\ e_{\hat{i}}{}^{\phi}\end{pmatrix}=\begin{pmatrix}\frac{a^2+r^2}{\sqrt{\Delta\Sigma}} & 0 & 0 & -\frac{a\sin\theta}{\sqrt{\Sigma}}\\ 0 & \sqrt{\frac{\Delta}{\Sigma}} & 0 & 0\\ \frac{a}{\sqrt{\Delta\Sigma}} & 0 & 0 & -\frac{\csc\theta}{\sqrt{\Sigma}}\\ 0 & 0 & -\sqrt{\frac{1}{\Sigma}} & 0\end{pmatrix}\begin{pmatrix}\lambda_{\hat{i}}{}^{t}\\ \lambda_{\hat{i}}{}^{r}\\ \lambda_{\hat{i}}{}^{\theta}\\ \lambda_{\hat{i}}{}^{\phi}\end{pmatrix}. \tag{A17}$$

The parameter Ψ is achieved via integrating the following equation in terms of (r, θ, ϕ) from (the radius of Earth, π/2, - π) to (the altitudes of orbits, π, π) with the intervals (100km, π /10, π /20).

$$\frac{d\psi}{d\xi}=\frac{K^{1/2}}{\Sigma}\left(\frac{E\left(r^2+a^2\right)-a\Phi}{r^2+K}+a\frac{\left(\Phi-aE\sin^2\theta\right)}{K-a^2\cos^2\theta}\right). \tag{A18}$$

These tetrads $\left(e_{\hat{t}}{}^{\mu}\partial_{\mu},e_{\hat{r}}{}^{\mu}\partial_{\mu},e_{\hat{\theta}}{}^{\mu}\partial_{\mu},e_{\hat{\phi}}{}^{\mu}\partial_{\mu}\right)$ are asymptotically parallel to the unit vectors of global coordinates $\left(\partial_t,\partial_r,\partial_\theta,\partial_\phi\right)$ as r goes to infinity. For equatorial orbits, r and θ should be constant, and thus Eq. 15 can be rewritten as

$$\frac{d\psi}{d\phi}=\frac{K^{1/2}}{\Sigma}\left(\frac{E\left(r^2+a^2\right)-a\Phi}{r^2+K}+a\frac{\left(\Phi-aE\sin^2\theta\right)}{K-a^2\cos^2\theta}\right)\frac{d\xi}{d\phi} \tag{A19}$$

For polar orbits, since θ is not constant and Eq. 15 is independent of ϕ, Ψ should be independent of ϕ. Otherwise, $d\Psi/d\xi$ becomes dependent on ϕ which is contradiction to the Eq. 15. Thus, we use the following equation for polar orbits:

$$\frac{d\psi}{d\theta}=\frac{K^{1/2}}{\Sigma}\left(\frac{E\left(r^2+a^2\right)-a\Phi}{r^2+K}+a\frac{\left(\Phi-aE\sin^2\theta\right)}{K-a^2\cos^2\theta}\right)\frac{d\xi}{d\theta} \qquad \text{(A20)}$$

A2. Wigner Rotation Angle

A Hermitian matrix K can be mapped to a wave vector k of the photon such that[2,3]

$$K=\sigma_a k^a\,, \qquad \text{(A21)}$$

where σ_0 is the 2x2 Identity matrix, and σ_i (i=1, 2, 3) are the Pauli matrices. Thus, K has the form[2,3]

$$K=k^{\hat{0}}\begin{pmatrix}1+n^{\hat{3}} & n^{\hat{1}}-in^{\hat{2}}\\ n^{\hat{1}}+in^{\hat{2}} & 1-n^{\hat{3}}\end{pmatrix}, \qquad \text{(A22)}$$

where $n^i=\dfrac{k^i}{k^0}\ (i=1,\,2,\,3)$. Also, a Lorentz transformation is described in the space of two-dimensional Hermitian matrices by a matrix A in SL(2, C) such that

$$.\quad K'=\Lambda^a{}_b k^b\sigma_a=AKA^\dagger \qquad \text{(A23)}$$

The Wigner's little group element[2-4], $W(\Lambda,k)=L^{-1}_{\Lambda k}\Lambda L_k$, is then given by

$$S(\Lambda,k)=A^{-1}{}_{k'}AA_k\,, \qquad \text{(A24)}$$

where A_k corresponds to $L(k)$ that transforms $\tilde{k} = (1,0,0,1)$ into k. It is straightforward to show the $S(\Lambda,k)$ has the form [3]:

$$S = \begin{pmatrix} e^{i\psi/2} & z \\ 0 & e^{-i\psi/2} \end{pmatrix}, \qquad \psi \in [0, 4\pi], \tag{A25}$$

and the A_k has the form

$$. \qquad A_k = \frac{1}{\sqrt{2k^{\hat{0}}(1+n^{\hat{3}})}} \begin{pmatrix} k^{\hat{0}}(1+n^{\hat{3}}) & -n_- \\ k^{\hat{0}} n_+ & 1+n^{\hat{3}} \end{pmatrix}. \tag{A26}$$

A Lorentz transformed wave vector, $k' = \Lambda k$, is mapped to a Hermitian matrix K' given by

$$K' = k'^{\hat{0}} \begin{pmatrix} 1+n'^{\hat{3}} & n'_- \\ n'_+ & 1-n'^{\hat{3}} \end{pmatrix} = \mathrm{AKA}^{\dagger} = k^0 \begin{pmatrix} b & c^* \\ c & a-b \end{pmatrix}, \tag{A27}$$

where $A = \begin{pmatrix} \alpha & \beta \\ \gamma & \delta \end{pmatrix} \in SL(2,C)$. Then we can get the following relations

$$\begin{aligned} a = (|\alpha|^2 + |\gamma|^2)(1+\mathrm{n}^3) + (|\beta|^2 + |\delta|^2)(1-\mathrm{n}^3) \\ + (\alpha\beta^* + \gamma\delta^*)\,\mathrm{n}_- + (\alpha^*\beta + \gamma^*\delta)\,\mathrm{n}_+ \end{aligned} \tag{A28}$$

$$b = |\alpha|^2 (1+\mathrm{n}^3) + |\beta|^2 (1-\mathrm{n}^3) + \alpha\beta^*\,\mathrm{n}_- + \alpha^*\beta\,\mathrm{n}_+ \tag{A29}$$

$$c = \alpha^*\gamma(1+\mathrm{n}^3) + \beta^*\delta(1-\mathrm{n}^3) + \beta^*\gamma\,\mathrm{n}_- + \alpha^*\delta\,\mathrm{n}_+ \tag{A30}$$

$$k'^{\hat{0}} = \frac{a}{2} k^{\hat{0}}, \quad n'^{\hat{3}} = \frac{2b}{a} - 1, \quad n'_+ = \frac{2c}{a} \tag{A31}$$

Here, z is an arbitrary complex number. Substituting from Eq. A25 to Eq. A31 into Eq. A24, we can get the relation[2]

$$e^{i(\psi(\Lambda,\mathrm{k})/2)}=\frac{[\alpha(1+\mathrm{n}^{\hat{3}})+\beta\,\mathrm{n}_{+}]b+[\gamma(1+\mathrm{n}^{\hat{3}})+\delta\,\mathrm{n}_{+}]c^{*}}{a\sqrt{b(1+\mathrm{n}^{\hat{3}})}}. \qquad \text{(A32)}$$

Moreover, by redefining the z, the matrix S can be given in the form[3]

$$S=\begin{pmatrix} e^{i\psi/2} & e^{-i\psi/2}z \\ 0 & e^{-i\psi/2}z \end{pmatrix},\quad \psi\in[0,4\pi], \qquad \text{(A33)}$$

and the product of any two elements in this group

$$S_1S_2=\begin{pmatrix} e^{i(\psi_1+\psi_2)/2} & e^{-i(\psi_1+\psi_2)/2}(z_1+e^{i\psi_1}\,\mathrm{z}_2) \\ 0 & e^{-i(\psi_1+\psi_2)/2} \end{pmatrix},\quad \psi\in[0,4\pi] \qquad \text{(A34)}$$

In other words, we have the following composition law such that

$$.\quad (\mathrm{z}_1,\psi_1)(\mathrm{z}_2,\psi_2)=(\mathrm{z}_1+\exp(i\psi_1)\,\mathrm{z}_2,\psi_1+\psi_2) \qquad \text{(A35)}$$

Thus, for massless particles, Wigner's little group is the E(2) group. There are two classes of the irreducible unitary representations of the E(2). One is the infinitesimal dimension representations, and the other is the one-dimension representation. However, the former has intrinsic continuous degrees of freedom. Therefore, the Lorentz transformation for the photon has the one-dimension representations, since the photon is not observed to have any continuous degrees of freedom. The representations have the form[4]

$$U(\Lambda)\left|k,\sigma\right\rangle=\mathrm{e}^{i\sigma\psi(\Lambda,k)}\left|\Lambda k,\sigma\right\rangle. \qquad \text{(A36)}$$

Here, $\psi(\Lambda,\mathrm{k})$ is the Wigner angle. When equation (S26) is expanded to the first order of $d\xi$ in the form

$$e^{i\psi(\Lambda,k)/2}\sim 1+i\tilde{\psi}(\Lambda,k)\frac{d\xi}{2}, \qquad \text{(A37)}$$

the total Wigner rotations can be built up as a time-ordered integration of

infinitesimal Wigner rotations over the geodesic trajectory x(ξ) of the photon via

$$e^{i\psi(\Lambda,\vec{n})/2} = T\exp\left[i\int\tilde{\psi}(\Lambda(\xi),\vec{n}(\xi))\frac{d\xi}{2}\right], \tag{A38}$$

where $\vec{n}(\xi)=\vec{n}(\mathrm{x}(\xi)), \Lambda^{\mu}{}_{\nu}(\xi)=\Lambda^{\mu}{}_{\nu}(\mathrm{x}(\xi))$ and T is the time order operator. For the infinitesimal homogeneous Lorentz transformation expanded as $\Lambda^{\hat{a}}{}_{\hat{b}}=\delta^{\hat{a}}{}_{\hat{b}}+\lambda^{\hat{a}}{}_{\hat{b}}$ with the Kronecker delta $\delta^{\hat{a}}{}_{\hat{b}}$ and infinitesimal boosts and rotations $\lambda^{\hat{a}}{}_{\hat{b}}$., we expand A in terms of dξ as

$$A=\begin{pmatrix}\alpha & \beta\\ \gamma & \delta\end{pmatrix}=I+\tilde{A}\mathrm{d}\xi=I+\begin{pmatrix}\tilde{\alpha} & \tilde{\beta}\\ \tilde{\gamma} & \tilde{\delta}\end{pmatrix}\mathrm{d}\xi \tag{A39}$$

From the condition that the A has unit determinant, it is obtained that $\tilde{\delta}=-\tilde{\alpha}$. Thus, the A can be rewritten as:

$$A=\begin{pmatrix}\alpha & \beta\\ \gamma & \delta\end{pmatrix}=I+\tilde{A}d\xi=I+\begin{pmatrix}\tilde{\alpha} & \tilde{\beta}\\ \tilde{\gamma} & -\tilde{\alpha}\end{pmatrix}d\xi\,. \tag{A40}$$

Substituting Eq. S40 into Eq. S23, multiplying $\sigma_{\hat{a}}$, and taking a trace on both sides, we can get the following equations

$$\lambda^{\hat{a}}{}_{\hat{b}}=\frac{1}{2}\delta^{\hat{a}\hat{c}}tr(\sigma_{\hat{b}}\sigma_{\hat{c}}\tilde{A}+\sigma_{\hat{c}}\sigma_{\hat{b}}\tilde{A}^{\dagger})\,, \tag{A41}$$

where tr(A) is the trace of A, and $\tilde{\alpha}$, $\tilde{\beta}$, and $\tilde{\gamma}$ are as follows:

$$\tilde{\alpha} = \frac{1}{2}(\lambda^{\hat{0}}{}_{\hat{3}} + \mathrm{i}\,\lambda^{\hat{1}}{}_{\hat{2}})$$
$$\tilde{\beta} = \frac{1}{2}[(\lambda^{\hat{0}}{}_{\hat{1}} + \lambda^{\hat{3}}{}_{\hat{1}}) + \mathrm{i}(-\lambda^{\hat{0}}{}_{\hat{2}} + \lambda^{\hat{2}}{}_{\hat{3}})] \qquad \text{(A42)}$$
$$\tilde{\gamma} = \frac{1}{2}[(\lambda^{\hat{0}}{}_{\hat{1}} - \lambda^{\hat{3}}{}_{\hat{1}}) + \mathrm{i}(\lambda^{\hat{0}}{}_{\hat{2}} + \lambda^{\hat{2}}{}_{\hat{3}})].$$

A4. Real parameters

The $\alpha, \beta, \gamma, \delta,$ and their moduli have the following forms:

$$\begin{cases} \alpha = 1 + \tilde{\alpha} d\xi \\ \beta = \tilde{\beta} d\xi \\ \gamma = \tilde{\gamma} d\xi \\ \delta = 1 - \tilde{\alpha} d\xi \end{cases} \text{ and } \begin{cases} |\alpha|^2 = 1 + 2\tilde{\alpha} d\xi \\ |\beta|^2 = 0 \\ |\gamma|^2 = 0 \\ |\delta|^2 = 1 - 2\tilde{\alpha} d\xi \end{cases}. \qquad \text{(A43)}$$

For photon moving in the $\hat{1} - \hat{2}$ plane, substituting Eq. S43 and $n_{\pm} = n^{\hat{1}}$ into Eqs. A28, A29 and A30, we obtain

$$a = 2 + 2(2\tilde{\alpha} n^{\hat{3}} + (\tilde{\beta} + \tilde{\gamma})\mathrm{n}^{\hat{1}}) d\xi, \qquad \text{(A44)}$$

$$b = (1 + \mathrm{n}^{\hat{3}}) + 2\left(2\tilde{\alpha}(1 + \mathrm{n}^{\hat{3}}) + \tilde{\beta} n^{\hat{1}}\right) d\xi, \qquad \text{(S45)}$$

and

$$c = n^{\hat{1}} + \left(\tilde{\gamma}(1 + \mathrm{n}^{\hat{3}}) + \tilde{\beta}(1 - \mathrm{n}^{\hat{3}})\right) d\xi. \qquad \text{(A46)}$$

The numerator of Eq. A32 is given in terms of the parameters defined above:

$$
\begin{aligned}
&[\alpha(1+\mathrm{n}^{\hat{3}})+\beta\,\mathrm{n}_{+}]\mathrm{b}+[\gamma(1+\mathrm{n}^{\hat{3}})+d\,\mathrm{n}_{+}]\mathrm{c}^{*} \\
&=2(1+\mathrm{n}^{\hat{3}}) \\
&\quad+\begin{bmatrix} 2\tilde{\alpha}+6\tilde{\alpha}n^{\hat{3}}+4\alpha(n^{\hat{3}})^{2}+4\beta n^{\hat{1}} \\ +2\beta n^{\hat{1}}n^{\hat{3}}+2\tilde{\gamma}n^{\hat{1}}+2\tilde{\gamma}n^{\hat{1}}n^{\hat{3}} \end{bmatrix} d\xi,
\end{aligned}
\tag{A47}
$$

and the denominator is

$$
\begin{aligned}
&\frac{1}{a\sqrt{b(1+\mathrm{n}^{\hat{3}})}} \\
&=\frac{1}{2(1+\mathrm{n}^{\hat{3}})}-\frac{2\tilde{\alpha}n^{\hat{3}}+\tilde{\beta}n^{\hat{1}}+\tilde{\gamma}n^{\hat{1}}+2\tilde{\alpha}+2\tilde{\beta}n^{\hat{1}}(1+\mathrm{n}^{\hat{3}})^{-1}}{2(1+\mathrm{n}^{\hat{3}})}d\xi
\end{aligned}
\tag{A48}
$$

By direct calculations, one can show that Eq. A32 becomes

$$
e^{i(\psi(\Lambda,\mathrm{k})/2)}=1. \tag{A49}
$$

A6. Complex parameters

In the case that every parameter is not real, $|\alpha|^{2},|\beta|^{2},|\gamma|^{2},|\delta|^{2}$ have the form

$$
\begin{aligned}
|\alpha|^{2}&=1+2\,\mathrm{Re}(\tilde{\alpha})d\xi \\
|\beta|^{2}&=0 \\
|\gamma|^{2}&=0 \\
|\delta|^{2}&=1-2\,\mathrm{Re}(\tilde{\alpha})d\xi,
\end{aligned}
\tag{A50}
$$

where $\mathrm{Re}(\bullet)$ is the real part of the complex number $\bullet$. Eqs. S44, S45, and S46 are then rewritten

$$
\begin{aligned}
a&=(|\alpha|^{2}+|\gamma|^{2})(1+\mathrm{n}^{3})+(|\beta|^{2}+|\delta|^{2})(1-\mathrm{n}^{3}) \\
&\quad+(\alpha\beta^{*}+\gamma\delta^{*})\,\mathrm{n}_{-}+(\alpha^{*}\beta+\gamma^{*}\delta)\,\mathrm{n}_{+} \\
&=2+[4n^{3}\,\mathrm{Re}(\tilde{\alpha})+2\,\mathrm{Re}(\tilde{\beta}\,\mathrm{n}_{+}+\tilde{\gamma}\,\mathrm{n}_{-})]d\xi,
\end{aligned}
\tag{A51}
$$

$$
\begin{aligned}
b &= |\alpha|^2 (1+\mathrm{n}^{\hat{3}}) + |\beta|^2 (1-\mathrm{n}^{\hat{3}}) + \alpha\beta^* \mathrm{n}_- + \alpha^* \beta \mathrm{n}_+ \\
&= \left(1 + 2\,\mathrm{Re}(\tilde{\alpha}) d\xi\right)(1+\mathrm{n}^{\hat{3}}) + 2\,\mathrm{Re}(\tilde{\beta}\,\mathrm{n}_+)\,\mathrm{d}\,\xi \\
&= (1+\mathrm{n}^{\hat{3}}) + [2\,\mathrm{Re}(\tilde{\alpha})(1+\mathrm{n}^{\hat{3}}) + 2\,\mathrm{Re}(\tilde{\beta}\,\mathrm{n}_+)]\,\mathrm{d}\,\xi,
\end{aligned}
\tag{A52}
$$

and

$$
\begin{aligned}
c &= \alpha^* \gamma (1+\mathrm{n}^{\hat{3}}) + \beta^* \delta (1-\mathrm{n}^{\hat{3}}) + \beta^* \gamma\, \mathrm{n}_- + \alpha^* \delta\, \mathrm{n}_+ \\
&= \tilde{\gamma}(1+\mathrm{n}^{\hat{3}})\,\mathrm{d}\,\xi + \tilde{\beta}^*(1-\mathrm{n}^{\hat{3}})\,\mathrm{d}\,\xi + \left(1+\tilde{\alpha}^* d\xi\right)\left(1-\tilde{\alpha} d\xi\right)\mathrm{n}_+ \\
&= \mathrm{n}_+ + [\tilde{\gamma}(1+\mathrm{n}^{\hat{3}}) + \tilde{\beta}^*(1-\mathrm{n}^{\hat{3}}) - 2i\,\mathrm{n}_+\,\mathrm{Im}(\tilde{\alpha})]\,\mathrm{d}\,\xi.
\end{aligned}
\tag{A53}
$$

, where Im(•) is the imaginary part of complex numbers. Thus, with Eqs. S51, S52, and S53, we obtain

$$
\begin{aligned}
&[\alpha(1+\mathrm{n}^{\hat{3}}) + \beta\,\mathrm{n}_+]\mathrm{b} + [\gamma(1+\mathrm{n}^{\hat{3}}) + \delta\,\mathrm{n}_+]\mathrm{c}^* \\
&= ((1+\mathrm{n}^{\hat{3}}) + [\tilde{\alpha}(1+\mathrm{n}^{\hat{3}}) + \tilde{\beta}\,\mathrm{n}_+] d\xi) \\
&\quad ((1+\mathrm{n}^{\hat{3}}) + [2\,\mathrm{Re}(\tilde{\alpha})(1+\mathrm{n}^{\hat{3}}) + 2\,\mathrm{Re}(\tilde{\beta}\,\mathrm{n}_+)]\,\mathrm{d}\,\xi) \\
&\quad + (n_+ + [\tilde{\gamma}(1+\mathrm{n}^{\hat{3}}) - \tilde{\alpha}\,\mathrm{n}_+] d\xi)(\mathrm{n}_- + [\tilde{\gamma}^*(1+\mathrm{n}^{\hat{3}}) \\
&\quad + \tilde{\beta}(1-\mathrm{n}^{\hat{3}}) + 2i n_-\,\mathrm{Im}(\tilde{\alpha})]\,\mathrm{d}\,\xi) \\
&= (1+\mathrm{n}^{\hat{3}})^2 + n_+\,\mathrm{n}_- \\
&\quad + \begin{bmatrix} \tilde{\alpha}(1+\mathrm{n}^{\hat{3}})^2 + \tilde{\beta}\,\mathrm{n}_+(1+\mathrm{n}^{\hat{3}}) + 2\,\mathrm{Re}(\tilde{\alpha})(1+\mathrm{n}^{\hat{3}})^2 \\ +2\,\mathrm{Re}(\tilde{\beta}\,\mathrm{n}_+)(1+\mathrm{n}^{\hat{3}}) - \tilde{\alpha}\,\mathrm{n}_+\mathrm{n}_- + 2\,\mathrm{Re}(\tilde{\gamma}^* n_+)(1+\mathrm{n}^{\hat{3}}) \\ +\tilde{\beta} n_+(1-\mathrm{n}^{\hat{3}}) + 2i n_+\,\mathrm{n}_-\,\mathrm{Im}(\tilde{\alpha}) \end{bmatrix} d\xi \\
&= 2(1+\mathrm{n}^{\hat{3}}) + \begin{bmatrix} 2\tilde{\alpha}\,\mathrm{n}^{\hat{3}}(1+\mathrm{n}^{\hat{3}}) + 2\tilde{\beta}\,\mathrm{n}_+ + 2\,\mathrm{Re}(\tilde{\alpha})(1+\mathrm{n}^{\hat{3}})^2 \\ +2\,\mathrm{Re}(\tilde{\beta}\,\mathrm{n}_+)(1+\mathrm{n}^{\hat{3}}) + \mathrm{Re}(\tilde{\gamma}^* n_+)(1+\mathrm{n}^{\hat{3}}) \\ +2i n_+\,\mathrm{n}_-\,\mathrm{Im}(\tilde{\alpha}) \end{bmatrix} d\xi \\
&= 2(1+\mathrm{n}^{\hat{3}}) \left(1 + \frac{1}{2(1+\mathrm{n}^{\hat{3}})} \begin{bmatrix} 2\tilde{\alpha}\,\mathrm{n}^{\hat{3}}(1+\mathrm{n}^{\hat{3}}) + 2\tilde{\beta}\,\mathrm{n}_+ + 2\,\mathrm{Re}(\tilde{\alpha})(1+\mathrm{n}^{\hat{3}})^2 \\ +2\,\mathrm{Re}(\tilde{\beta}\,\mathrm{n}_+)(1+\mathrm{n}^{\hat{3}}) + \mathrm{Re}(\tilde{\gamma}^* n_+)(1+\mathrm{n}^{\hat{3}}) \\ +2i n_+\,\mathrm{n}_-\,\mathrm{Im}(\tilde{\alpha}) \end{bmatrix} d\xi \right)
\end{aligned}
\tag{A54}
$$

and

$$\frac{1}{a\sqrt{b(1+\hat{n}^3}}$$

$$=\left(\frac{1}{2+[4\hat{n}^3\,\mathrm{Re}(\tilde{\alpha})+2\,\mathrm{Re}(\tilde{\beta}\,n_{+}+\tilde{\gamma}\,n_{-})]d\xi}\right)$$

$$\left(\frac{1}{\sqrt{(1+\hat{n}^3)^2+[2\,\mathrm{Re}(\tilde{\alpha})(1+\hat{n}^3)^2+2\,\mathrm{Re}(\tilde{\beta}\,n_{+})(1+\hat{n}^3)]\,d\,\xi}}\right)$$

$$=\frac{1}{2}\left(1-\frac{[4n^3\,\mathrm{Re}(\tilde{\alpha})+2\,\mathrm{Re}(\tilde{\beta}\,n_{+}+\tilde{\gamma}\,n_{-})]}{2}d\xi\right)$$

$$\left(\frac{1}{(1+\hat{n}^3)}\frac{1}{\sqrt{\frac{1+[2\,\mathrm{Re}(\tilde{\alpha})(1+\hat{n}^3)+2\,\mathrm{Re}(\tilde{\beta}\,n_{+})]\,d\,\xi}{(1+\hat{n}^3)}}}\right)$$

$$=\frac{1}{2(1+\hat{n}^3)}\left(1-\frac{[4n^3\,\mathrm{Re}(\tilde{\alpha})(1+\hat{n}^3)+2\,\mathrm{Re}(\tilde{\beta}\,n_{+}+\tilde{\gamma}\,n_{-})(1+\hat{n}^3)]}{2(1+\hat{n}^3)}d\xi\right) \quad \text{(A55)}$$

$$\left(1-\frac{[2\,\mathrm{Re}(\tilde{\alpha})(1+\hat{n}^3)+2\,\mathrm{Re}(\tilde{\beta}\,n_{+})]}{2(1+\hat{n}^3)}d\xi\right).$$

Substituting these results into Eq. A32, we have the form

$$
\begin{aligned}
e^{i(\psi(\Lambda,\mathrm{k})/2)} &= \frac{[\alpha(1+\hat{\mathrm{n}}^3)+\beta\,\mathrm{n}_+]\mathrm{b}+[\gamma(1+\hat{\mathrm{n}}^3)+\delta\,\mathrm{n}_+]\mathrm{c}^*}{a\sqrt{b(1+\hat{\mathrm{n}}^3)}} \\
&= \left(1-\frac{[4\hat{\mathrm{n}}^3\,\mathrm{Re}(\tilde{\alpha})(1+\hat{\mathrm{n}}^3)+2\,\mathrm{Re}(\tilde{\beta}\,\mathrm{n}_+ +\tilde{\gamma}\,\mathrm{n}_-)(1+\hat{\mathrm{n}}^3)]}{2(1+\hat{\mathrm{n}}^3)}d\xi\right) \\
&\quad \left(1-\frac{[2\,\mathrm{Re}(\tilde{\alpha})(1+\hat{\mathrm{n}}^3)+2\,\mathrm{Re}(\tilde{\beta}\,\mathrm{n}_+)]}{2(1+\hat{\mathrm{n}}^3)}d\xi\right) \\
&\left(1+\left[\begin{array}{l}\dfrac{2\tilde{\alpha}\,\hat{\mathrm{n}}^3(1+\hat{\mathrm{n}}^3)+2\tilde{\beta}\,\mathrm{n}_+ +2\,\mathrm{Re}(\tilde{\alpha})(1+\hat{\mathrm{n}}^3)^2}{2(1+\hat{\mathrm{n}}^3)}d\xi \\ +\dfrac{2\,\mathrm{Re}(\tilde{\beta}\,\mathrm{n}_+)(1+\hat{\mathrm{n}}^3)+\mathrm{Re}(\tilde{\gamma}^* n_+)(1+\hat{\mathrm{n}}^3)+2i n_+\,\mathrm{n}_-\,\mathrm{Im}(\tilde{\alpha})}{2(1+\hat{\mathrm{n}}^3)}d\xi\end{array}\right]\right) \\
&= 1+\frac{1}{2(1+\hat{\mathrm{n}}^3)}\left[\begin{array}{l}-4\hat{\mathrm{n}}^3\,\mathrm{Re}(\tilde{\alpha})(1+\hat{\mathrm{n}}^3) \\ -2\,\mathrm{Re}(\tilde{\beta}\,\mathrm{n}_+ +\tilde{\gamma}\,\mathrm{n}_-)(1+\hat{\mathrm{n}}^3)-2\,\mathrm{Re}(\tilde{\alpha})(1+\hat{\mathrm{n}}^3) \\ -2\,\mathrm{Re}(\tilde{\beta}\,\mathrm{n}_+)+2\tilde{\alpha}\,\hat{\mathrm{n}}^3(1+\hat{\mathrm{n}}^3)+2\tilde{\beta}\,\mathrm{n}_+ \\ +2\,\mathrm{Re}(\tilde{\alpha})(1+\hat{\mathrm{n}}^3)^2+2\,\mathrm{Re}(\tilde{\beta}\,\mathrm{n}_+)(1+\hat{\mathrm{n}}^3) \\ +\mathrm{Re}(\tilde{\gamma}^* n_+)(1+\hat{\mathrm{n}}^3)+2i n_+\,\mathrm{n}_-\,\mathrm{Im}(\tilde{\alpha})\end{array}\right]d\xi \\
&= 1+\frac{1}{2(1+\hat{\mathrm{n}}^3)}\left[\begin{array}{l}-2\,\mathrm{Re}(\tilde{\beta}\,\mathrm{n}_+ +\tilde{\gamma}\,\mathrm{n}_-)(1+\hat{\mathrm{n}}^3)-2\,\mathrm{Re}(\tilde{\beta}\,\mathrm{n}_+) \\ +2\tilde{\beta}\,\mathrm{n}_+ +2\,\mathrm{Re}(\tilde{\beta}\,\mathrm{n}_+)(1+\hat{\mathrm{n}}^3) \\ +\mathrm{Re}(\tilde{\gamma}^* n_+)(1+\hat{\mathrm{n}}^3)+2i(1+\hat{\mathrm{n}}^3)\,\mathrm{Im}(\tilde{\alpha})\end{array}\right]d\xi.
\end{aligned}
\tag{A56}
$$

Since the real component of the parameters in Eq. A32 leads to unity, as seen in the previous section, Eq. A56 can be written as

$$
\begin{aligned}
&\frac{1}{a\sqrt{b(1+\hat{\mathrm{n}}^3)}}[\alpha(1+\hat{\mathrm{n}}^3)+\beta\,\mathrm{n}_+]\mathrm{b}+[\gamma(1+\hat{\mathrm{n}}^3)+d\,\mathrm{n}_+]\mathrm{c}^* \\
&\quad = 1+i[\mathrm{Re}(\tilde{\beta})\frac{\hat{\mathrm{n}}^2}{1+\hat{\mathrm{n}}^3}+\mathrm{Im}(\tilde{\beta})\frac{\hat{\mathrm{n}}^1}{1+\hat{\mathrm{n}}^3}+\mathrm{Im}(\tilde{\alpha})]d\xi.
\end{aligned}
\tag{A57}
$$

By definition, the infinitesimal Wigner angle is

$$\tilde{\psi} = 2\,\mathrm{Im}(\tilde{\alpha}) + \frac{2n^{\hat{1}}}{1+n^{\hat{3}}}\,\mathrm{Im}(\tilde{\beta}) + \frac{2n^{\hat{2}}}{1+n^{\hat{3}}}\,\mathrm{Re}(\tilde{\beta}). \tag{A58}$$

A7. Tetrads for a stationary observer

The tetrads, $e_{\hat{a}}{}^{\mu}(x)$, are defined as[5,6]

$$g_{\mu\nu}(x) e_{\hat{a}}{}^{\mu}(x) \cdot e_{\hat{b}}{}^{\nu}(x) = \eta_{\hat{a}\hat{b}} \tag{A59}$$

For a stationary observer, his local frame is defined in Schwarzschild spacetime such that,

$$\begin{aligned}
(e_{\hat{0}})^{\mu}(x) &= (e_t)^{\mu}(x) = (1/(1-r_s/\mathrm{r})^{1/2}, 0, 0, 0) \\
(e_{\hat{1}})^{\mu}(x) &= (e_r)^{\mu}(x) = (0, (1-r_s/\mathrm{r})^{1/2}, 0, 0) \\
(e_{\hat{2}})^{\mu}(x) &= (e_\theta)^{\mu}(x) = (0, 0, 1/r, 0) \\
(e_{\hat{3}})^{\mu}(x) &= (e_\phi)^{\mu}(x) = (0, 0, 0, 1/r).
\end{aligned} \tag{A60}$$

The corresponding ILLT(Infinitesimal Local Lorentz Transformation) matrix is given by

$$\begin{aligned}
\lambda^{\hat{a}}{}_{\hat{b}}(x) &= \eta^{\hat{a}\hat{c}} \left(\nabla_{\mathbf{k}} e_{\hat{c}}{}^{\nu}(x)\right) e_{\nu}{}^{\hat{d}}(x) \eta_{\hat{d}\hat{b}} \\
&= \begin{pmatrix}
0 & -\frac{k^t r_s}{2r^2} & 0 & 0 \\
-\frac{k^t r_s}{2r^2} & 0 & 0 & k^{\phi}(1-\frac{r_s}{r})^{1/2} \\
0 & -k^{\phi}(1-\frac{r_s}{r})^{1/2} & 0 & 0 \\
0 & 0 & 0 & 0
\end{pmatrix}.
\end{aligned} \tag{A61}$$

All the parameters, defined in Eq. A43, are real with the ILLT matrix of static observers. Thus, observers at rest cannot see Wigner rotation.

A8. Tetrads for a free-falling observer with zero angular momentum

For observers falling radially inward, away from infinity, the observers' energy and angular momentum per rest mass, defined in Eq. A5, are 1 and 0, respectively. Thus, the timelike component of the 4-velocity vector is $(1-r_s/r)^{-1}$, and the ϕ- and θ-direction components of the 4-velocity vector are zero. Thus, 4-velocity vectors of the observers have the form:

$$-(1-\frac{r_s}{r})\left(\frac{dt}{d\xi}\right)^2+(1-\frac{r_s}{r})^{-1}\left(\frac{dr}{d\xi}\right)^2=-1. \qquad \text{(A62)}$$

Correspondingly, the observer's local frame can be described with the tetrads:

$$\begin{aligned}
&(e_{\hat{0}})^{\mu}(x)=(e_t)^{\mu}(x)=(1/(1-r_s/\mathrm{r}),-\sqrt{r_s/r},0,0)\\
&(e_{\hat{1}})^{\mu}(x)=(e_r)^{\mu}(x)=(\frac{\sqrt{r_s/r}}{1-r_s/r},1,0,0)\\
&(e_{\hat{2}})^{\mu}(x)=(e_\theta)^{\mu}(x)=(0,0,1/r,0)\\
&(e_{\hat{3}})^{\mu}(x)=(e_\phi)^{\mu}(x)=(0,0,0,1/r).
\end{aligned} \qquad \text{(A63)}$$

With this tetrads, the ILLT matrix is given by

$$(\lambda^{\hat{a}}{}_{\hat{b}})=\begin{pmatrix}
0 & -\frac{k^t r_s}{2r^2}-\sqrt{\frac{r_s}{r}}\frac{k^r}{2r(1-\frac{r_s}{r})} & 0 & -k^{\phi}\sqrt{\frac{r_s}{r}}\\
-\frac{k^t r_s}{2r^2}-\sqrt{\frac{r_s}{r}}\frac{k^r}{2\mathrm{r}(1-\frac{r_s}{r})} & 0 & k^{\phi} & 0\\
-k^{\phi}\sqrt{\frac{r_s}{r}} & -k^{\phi} & 0 & 0\\
0 & 0 & 0 & 0
\end{pmatrix}. \qquad \text{(A64)}$$

As the static case, since all the parameters are real, Wigner rotation is not observed in radially free-falling frames.

A9. Tetrads for a free-falling observer with non-zero angular momentum on circular orbits

By using a 4-velocity vector of an observer on stable circular orbit[1], we can get a corresponding tetrad such that

$$
\begin{aligned}
&(e_{\hat{0}})^{\mu}(x) = (e_{t})^{\mu}(x) = (\frac{1}{\sqrt{1-\frac{3r_s}{2r}}}, 0, \frac{1}{r}\sqrt{\frac{r_s}{2r}}\frac{1}{\sqrt{1-\frac{3r_s}{2r}}}, 0) \\
&(e_{\hat{1}})^{\mu}(x) = (e_{r})^{\mu}(x)(-\sqrt{\frac{r_s}{2r}}\frac{\sin\tilde{\Theta}(r)}{\sqrt{1-\frac{3r_s}{2r}}\sqrt{1-\frac{r_s}{r}}}, \sqrt{1-\frac{r_s}{r}}\cos\tilde{\Theta}(r), -\frac{1}{r}\frac{\sqrt{1-\frac{r_s}{r}}\sin\tilde{\Theta}(r)}{\sqrt{1-\frac{3r_s}{2r}}}, 0) \\
&(e_{\hat{2}})^{\mu}(x) = (e_{\theta})^{\mu}(x)(\sqrt{\frac{r_s}{2r}}\frac{\cos\tilde{\Theta}(r)}{\sqrt{1-\frac{3r_s}{2r}}\sqrt{1-\frac{r_s}{r}}}, \sqrt{1-\frac{r_s}{r}}\sin\tilde{\Theta}(r), \sqrt{1-\frac{r_s}{r}}, \frac{1}{r}\frac{\sqrt{1-\frac{r_s}{r}}\cos\tilde{\Theta}(r)}{\sqrt{1-\frac{3r_s}{2r}}}, 0) \\
&(e_{\hat{3}})^{\mu}(x) = (e_{\phi})^{\mu}(x) = (0, 0, 0, \csc\theta / r),
\end{aligned}
\tag{A65}
$$

and by applying non-spinning condition, we can get

$$
\tilde{\Theta}(r) = \sqrt{1-\frac{3r_s}{2r}}(\theta - \theta_0)\,. \tag{A66}
$$

Similar to the spiraling case, the tetrad of circular orbits is approximated up to the first order of $\sqrt{\frac{r_s}{r}}$ to figure out the physical meaning.

$$
\begin{aligned}
(e_{\hat{0}})^{\mu}(x) &= (e_{t})^{\mu}(x) = (1,0,\frac{1}{r}\sqrt{\frac{r_s}{2r}},0) \\
(e_{\hat{1}})^{\mu}(x) &= (e_{r})^{\mu}(x)(-\sqrt{\frac{r_s}{2r}}\sin(\theta-\theta_0),\cos(\theta-\theta_0),-\frac{1}{r}\sin(\theta-\theta_0),0) \\
(e_{\hat{2}})^{\mu}(x) &= (e_{\theta})^{\mu}(x)(\sqrt{\frac{r_s}{2r}}\cos(\theta-\theta_0),\sin(\theta-\theta_0),\frac{1}{r}\cos(\theta-\theta_0),0) \\
(e_{\hat{3}})^{\mu}(x) &= (e_{\phi})^{\mu}(x) = (0,0,0,\frac{\csc\theta}{r}).
\end{aligned}
\tag{A67}
$$

By projecting tetrads into 3-dimensional space, one can see that the tetrad is rotated by θ when the observer moves by $-r\theta$. This is a non-relativistic effect since the rotation induced by parallel transportation condition is just compensation of the rotation from the definition of spherical coordinates. In Fig. A1, it is shown that classical geodetic and residual components of IWRA for a free-falling observer with non-zero angular momentum in the circular orbit.

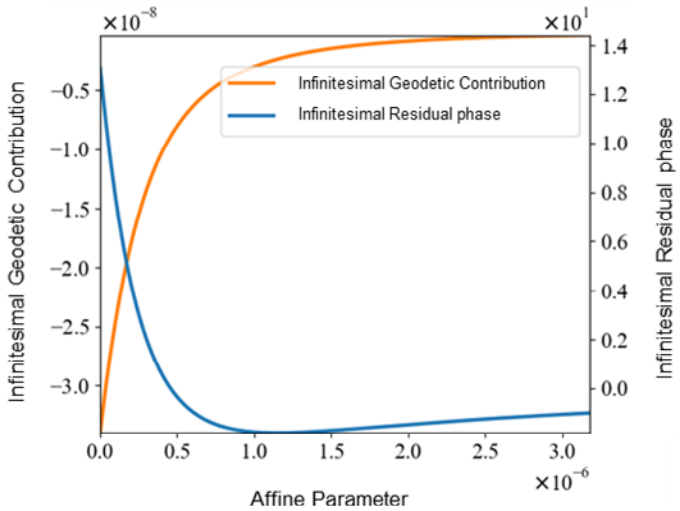

Fig. A1. Infinitesimal classical rotation and quantum rotation versus affine parameter for a free-falling observer with non-zero angular momentum in the circular orbit.

A10. Hong-Ou-Mandel effect with geometric phase

With creation operators of two input ports $a_{\mathrm{I}}^{\dagger}$ and $b_{\mathrm{I}}^{\dagger}$ and two output $c_{\mathrm{I}}^{\dagger}$ and $d_{\mathrm{I}}^{\dagger}$ of the first 50:50 beam splitter, the two indistinguishable photon states at each port can be written as

$$a^{\dagger}b^{\dagger}\left|0,0\right\rangle=\frac{1}{2}\left(c^{\dagger}+d^{\dagger}\right)\left(c^{\dagger}-d^{\dagger}\right)\left|0,0\right\rangle=\frac{1}{\sqrt{2}}c^{\dagger 2}\left|0,0\right\rangle-d^{\dagger 2}\left|0,0\right\rangle. \quad \text{(A68)}$$

Considering relative Wigner rotation angle at port c_{I} and $\pi/2$ phase shift at output port d_{I}, the photon states passing through output ports c_{II} and d_{II} of the second beam splitter

$$\begin{aligned}
&\frac{1}{\sqrt{2}}e^{\sigma i\Delta\psi}c_{\mathrm{I}}^{\dagger 2}\left|0,0\right\rangle-id_{\mathrm{I}}^{\dagger 2}\left|0,0\right\rangle\\
&=\frac{1}{2\sqrt{2}}e^{\sigma i\Delta\psi}\left(c_{\mathrm{II}}^{\dagger 2}+2c_{\mathrm{II}}^{\dagger}d_{\mathrm{II}}^{\dagger}+d_{\mathrm{II}}^{\dagger 2}\right)\left|0,0\right\rangle-\frac{i}{2\sqrt{2}}\left(c_{\mathrm{II}}^{\dagger 2}-2c_{\mathrm{II}}^{\dagger}d_{\mathrm{II}}^{\dagger}+d_{\mathrm{II}}^{\dagger 2}\right)\left|0,0\right\rangle\\
&=-i\left(\frac{ie^{\sigma i\psi}+1}{2\sqrt{2}}\left(c_{\mathrm{II}}^{\dagger 2}+d_{\mathrm{II}}^{\dagger 2}\right)+\frac{-1+ie^{\sigma i\psi}}{\sqrt{2}}c_{\mathrm{II}}^{\dagger}d_{\mathrm{II}}^{\dagger}\right)\left|0,0\right\rangle\\
&=-i\left(\frac{ie^{\sigma i\psi}+1}{2\sqrt{2}}\left(\left|2,0\right\rangle_{c_{\mathrm{II}}d_{\mathrm{II}}}+\left|0,2\right\rangle_{c_{\mathrm{II}}d_{\mathrm{II}}}\right)+\frac{-1+ie^{\sigma i\psi}}{\sqrt{2}}\left|1,1\right\rangle_{c_{\mathrm{II}}d_{\mathrm{II}}}\right).
\end{aligned} \quad \text{(A69)}$$

Table A1. Comparision of the geodetic precession calculated with tetrads on circular orbits and experimental results reported by

Geodetic precession calculated w/ tetrads on circular orbits	**Experimental results reported by C.W.F.Everitt et al.[7]**
6.6 arcsec/ *yr*	6.6018 ± 3 arcsec/yr

Table A2. Comparison of total integrated Wigner rotation angle (WRA) ψ_{total}, classical contribution to the WRA $\psi_{\text{total}}^{\text{geodetic}}$, and quantum contribution to the WRA $\psi_{\text{total}}^{\text{residual}}$ (in deg), for *radially emitted photons* and a satellite at various altitudes for circular orbits.

Observer in a Circular Orbit			
Altitude	**Wigner rotation angle (WRA) (classical part + residual part)** ψ_{total}	**Classical Part of the WRA** $\psi_{\text{total}}^{\text{geodetic}}$	**Residual Part of the WRA** $\psi_{\text{total}}^{\text{residual}}$
300km (NEO)	-3.44×10^{-5}	-4.67×10^{-14}	-3.44×10^{-5}
2000km (LEO)	-1.93×10^{-4}	-2.53×10^{-13}	-1.93×10^{-4}
20000km (MEO)	-7.77×10^{-4}	-6.17×10^{-13}	-7.77×10^{-4}
36000km (GEO)	-9.25×10^{-4}	-6.59×10^{-13}	-9.25×10^{-4}
$\mathbf{1.6\times10^{11}}$ **km** $(r=\infty)$	-1.51×10^{-3}	-7.00×10^{-13}	-1.51×10^{-3}

NEO, LEO, MEO and GEO = Near-, Low-, Medium- and Geosynchronous Earth

Bibliography

1 Yin, J. *et al.* Entanglement-based secure quantum cryptography over 1,120 kilometres. *Nature*, 1-5 (2020).

2 Yin, J. *et al.* Satellite-based entanglement distribution over 1200 kilometers. *Science* **356**, 1140, doi:10.1126/science.aan3211 (2017).

3 Ren, J.-G. *et al.* Ground-to-satellite quantum teleportation. *Nature* **549**, 70-73, doi:10.1038/nature23675 (2017).

4 Liao, S.-K. *et al.* Satellite-to-ground quantum key distribution. *Nature* **549**, 43-47, doi:10.1038/nature23655 (2017).

5 Liao, S.-K. *et al.* Satellite-Relayed Intercontinental Quantum Network. *Phys. Rev. Lett.* **120**, 030501, doi:10.1103/PhysRevLett.120.030501 (2018).

6 Buttler, W. T. *et al.* Free-space quantum-key distribution. *Physical Review A* **57**, 2379-2382, doi:10.1103/PhysRevA.57.2379 (1998).

7 Gibson, G. *et al.* Free-space information transfer using light beams carrying orbital angular momentum. *Opt. Express* **12**, 5448-5456, doi:10.1364/OPEX.12.005448 (2004).

8 Schmitt-Manderbach, T. *et al.* Experimental Demonstration of Free-Space Decoy-State Quantum Key Distribution over 144 km. *Physical Review Letters* **98**, 010504, doi:10.1103/PhysRevLett.98.010504 (2007).

9 Aolita, L. & Walborn, S. P. Quantum Communication without Alignment using Multiple-Qubit Single-Photon States. *Phys. Rev. Lett.* **98**, 100501, doi:10.1103/PhysRevLett.98.100501 (2007).

10 Laing, A., Scarani, V., Rarity, J. G. & O'Brien, J. L. Reference-frame-independent quantum key distribution. *Phys. Rev. A* **82**, 012304, doi:10.1103/PhysRevA.82.012304 (2010).

11 Zhang, P. *et al.* Reference-Frame-Independent Quantum-Key-Distribution Server with a Telecom Tether for an On-Chip Client. *Phys. Rev. Lett.* **112**, 130501, doi:10.1103/PhysRevLett.112.130501 (2014).

12 Erven, C. *et al.* Studying free-space transmission statistics and improving free-space quantum key distribution in the turbulent atmosphere. *New J. Phys.* **14**, 123018, doi:10.1088/1367-2630/14/12/123018 (2012).

13 Vallone, G. *et al.* Free-Space Quantum Key Distribution by Rotation-Invariant Twisted Photons. *Phys. Rev. Lett.* **113**, 060503, doi:10.1103/PhysRevLett.113.060503 (2014).

14 Yin, J. *et al.* Satellite-based entanglement distribution over 1200 kilometers. *Science* **356**, 1140-1144 (2017).

15 Liao, S.-K. *et al.* Satellite-to-ground quantum key distribution. *Nature* **549**, 43-47 (2017).

16 Ren, J.-G. *et al.* Ground-to-satellite quantum teleportation. *Nature* **549**, 70 (2017).

17 Armengol, J. M. P. *et al.* Quantum communications at ESA: towards a space experiment on the ISS. *Acta Astronautica* **63**, 165-178 (2008).

18 Ursin, R. *et al.* Space-quest, experiments with quantum entanglement in space. *Europhys. News* **40**, 26-29 (2009).

19 Rideout, D. *et al.* Fundamental quantum optics experiments conceivable with satellites—reaching relativistic distances and velocities. *Class Quantum Gravity* **29**, 224011 (2012).

20 Bruschi, D. E., Ralph, T. C., Fuentes, I., Jennewein, T. & Razavi, M. Spacetime effects on satellite-based quantum communications. *Phys. Rev. D* **90**, 045041 (2014).
21 Dowling, J. P. & Milburn, G. J. Quantum technology: the second quantum revolution. *Philos. Trans. Royal Soc. A* **361**, 1655-1674 (2003).
22 Takenaka, H. *et al.* Satellite-to-ground quantum-limited communication using a 50-kg-class microsatellite. *Nat. Photonics* **11**, 502-508, doi:10.1038/nphoton.2017.107 (2017).
23 Basso, M. L. W. & Maziero, J. Interferometric visibility in curved spacetimes. *Class Quantum Gravity* **38**, doi:10.1088/1361-6382/abfd84 (2021).
24 de Sitter, W. On Einstein's Theory of Gravitation and its Astronomical Consequences. Third Paper.⋆. *Mon. Notices Royal Astron. Soc.* **78**, 3-28, doi:10.1093/mnras/78.1.3 (1917).
25 Ahn, D. Black hole state evolution, final state and Hawking radiation. *Class Quantum Gravity* **29**, 224007 (2012).
26 Ahn, D. Unruh effect as a noisy quantum channel. *Phys. Rev. A* **98**, 022308 (2018).
27 PENROSE, R. & FLOYD, R. Extraction Rotational Energy from a Black Hole. *Nature Physical Science* **229**, 177-179, doi:https://doi.org/10.1038/physci229177a0 (1971).
28 Eduarte-Rojas, A., Frutos-Alfaro, F., Carboni, R. & Alvarado, D. Chaotic behavior of geodesics in Kerr-like spacetime. *Phys. Rev. D* **106**, doi:10.1103/PhysRevD.106.064015 (2022).
29 Schiff, L. I. Possible New Experimental Test of General Relativity Theory. *Phys. Rev. Lett.* **4**, 215-217, doi:10.1103/PhysRevLett.4.215 (1960).
30 Everitt, C. W. F. *et al.* Gravity Probe B: Final Results of a Space Experiment to Test General Relativity. *Phys. Rev. Lett.* **106**, 221101, doi:10.1103/PhysRevLett.106.221101 (2011).
31 Lense, J. & Thirring, H. Über den Einfluss der Eigenrotation der Zentralkörper auf die Bewegung der Planeten und Monde nach der Einsteinschen Gravitationstheorie. *PhyZ* **19**, 156 (1918).
32 Tamburini, F., Thidé, B., Molina-Terriza, G. & Anzolin, G. Twisting of light around rotating black holes. *Nature Physics* **7**, 195-197, doi:10.1038/nphys1907 (2011).
33 Kish, S. P. & Ralph, T. C. Quantum effects in rotating reference frames. *AVS Quantum Science* **4**, doi:10.1116/5.0073436 (2022).
34 Ohnuki, Y. *Unitary Representations of the Poincar Group and Relativistic Wave Equations*. (World Scientific, 1988).
35 Wigner, E. On unitary representations of the inhomogeneous Lorentz group. *Ann. Math.*, 149-204 (1939).
36 Weinberg, S. *The quantum theory of fields*. Vol. 1 (Cambridge university press, 1995).
37 Ahn, D., Lee, H.-j., Moon, Y. H. & Hwang, S. W. Relativistic entanglement and Bell's inequality. *Phys. Rev. A* **67**, 012103 (2003).
38 Nakahara, M. *Geometry, topology and physics*. (CRC Press, 2003).
39 Terashima, H. & Ueda, M. Einstein-Podolsky-Rosen correlation in a gravitational field. *Phys. Rev. A* **69**, 032113 (2004).
40 Ahn, D. Wigner rotation of a spin 1/2 particle near the event horizon of a schwarzschild black hole. *J Korean Phys Soc* **51**, 470-474 (2007).
41 Alsing, P. M., Stephenson Jr, G. J. & Kilian, P. Spin-induced non-

geodesic motion, gyroscopic precession, Wigner rotation and EPR correlations of massive spin 1/2 particles in a gravitational field. *arXiv preprint arXiv:0902.1396* (2009).
42 Alsing, P. M. & Stephenson Jr, G. J. The Wigner rotation for photons in an arbitrary gravitational field. *arXiv preprint arXiv:0902.1399* (2009).
43 Weinberg, S. Gravitation and cosmology: principles and applications of the general theory of relativity. (1972).
44 Brodutch, A. & Terno, D. R. Polarization rotation, reference frames, and Mach's principle. *Phys. Rev. D* **84**, 121501 (2011).
45 Noh, H., Alsing, P. M., Ahn, D., Miller, W. A. & Park, N. Quantum mechanical rotation of a photon polarization by Earth's gravitational field. *Npj Quantum Inf* **7**, doi:10.1038/s41534-021-00471-6 (2021).
46 Dahal, P. K. & Terno, D. R. Polarization rotation and near-Earth quantum communications. *Phys. Rev. A* **104**, doi:10.1103/PhysRevA.104.042610 (2021).
47 Hartle, J. B. (American Association of Physics Teachers, 2003).
48 Schwinger, J. Energy and Momentum Density in Field Theory. *Phys. Rev.* **130**, 800-805, doi:10.1103/PhysRev.130.800 (1963).
49 Misner, C. W., Thorne, K. S. & Wheeler, J. A. *Gravitation*. (Macmillan, 1973).
50 Caban, P. & Rembieliński, J. Photon polarization and Wigner's little group. *Phys. Rev. A* **68**, 042107 (2003).
51 Collaboration, E. H. T. *et al.* Gravitational Test beyond the First Post-Newtonian Order with the Shadow of the M87 Black Hole. *Phys. Rev. Lett.* **125**, 141104, doi:10.1103/PhysRevLett.125.141104 (2020).
52 De Felice, F. & Clarke, C. J. S. *Relativity on curved manifolds*. (Cambridge University Press, 1992).
53 Birrell, N. D. & Davies, P. C. W. Quantum Fields in Curved Space. (1982).
54 Kohlrus, J., Louko, J., Fuentes, I. & Bruschi, D. E. Wigner phase of photonic helicity states in the spacetime of the Earth. *arXiv preprint arXiv:1810.10502* (2018).
55 Chandrasekhar, S. & Thorne, K. S. *The mathematical theory of black holes*. (American Association of Physics Teachers, 1985).
56 Marck, J.-A. Solution to the equations of parallel transport in Kerr geometry; tidal tensor. *Proc. R. Soc. Lond. A* **385**, 431-438 (1983).
57 Sadana, S. *et al.* Near-100% two-photon-like coincidence-visibility dip with classical light and the role of complementarity. *Phys. Rev. A* **100**, doi:10.1103/PhysRevA.100.013839 (2019).
58 Roh, K.-M., Kopeikin, S. M. & Cho, J.-H. Numerical simulation of the post-Newtonian equations of motion for the near Earth satellite with an application to the LARES satellite. *Adv. Space Res.* **58**, 2255-2268 (2016).
59 Connors, P. A., Piran, T. & Stark, R. F. Polarization features of X-ray radiation emitted near black holes. *The Astrophysical Journal* **235**, 224-244 (1980).
60 Alsing, P. M. & Milburn, G. J. Teleportation with a uniformly accelerated partner. *Phys. Rev. Lett.* **91**, 180404 (2003).
61 Fuentes-Schuller, I. & Mann, R. B. Alice falls into a black hole: entanglement in noninertial frames. *Phys. Rev. Lett.* **95**, 120404 (2005).
62 Alsing, P. M., Fuentes-Schuller, I., Mann, R. B. & Tessier, T. E.

Entanglement of Dirac fields in noninertial frames. *Phys. Rev. A* **74**, 032326 (2006).
63 Hawking, S. W. Particle creation by black holes. *Commun. Math. Phys.* **43**, 199–220 (1975).
64 Unruh, W. G. Notes on black-hole evaporation. *Phys. Rev. D* **14**, 870 (1976).

요약(국문초록)

일반 상대론적 효과에 의한 광자의 기하학적 위상 변화

최근 위성으로 구성된 자유 공간 양자 광학 시스템의 발전으로 중력장에서 광자 상태의 evolution에 대한 조사가 널리 연구되었지만 대부분 proper time 연구에 국한되어왔다. 광자에 대해 로컬 프레임의 효과인 Wigner 회전을 다룬 몇 가지 선행 연구가 보고된 바 있으나, 이는 광자 궤적을 따라 고전적인 편광 벡터의 베리 위상으로 해석되어 왔다. 이 논문에서는 먼저 지구 중력장에 의해 유도된 기하학적 위상을 연구하기 위해 다양한 궤도의 관찰자 (인공위성)에 대해 Wigner 회전을 계산하였고 편광을 비교하기 위해 도입된 표준 프레임의 회전 외에도 측정 가능한 order의 Wigner 회전에 의한 위상이 있을 수 있음을 보였다. 이 Wigner 회전은 관찰자가 0이 아닌 각운동량을 갖는 경우인 원형 궤도를 따라 움직일 때, 지구 궤도의 고도에 따라 각각 10^{-6}도에서 10^{-4}도의 추가 위상을 가졌고 거의 0에 가까운 (10^{-12}도)측지 회전에대해 상대적으로 큰 값을 갖는 다는 것을 확인하였다. 또한 지구 근처의 극 궤도에있는 위성으로 구성된 2 광자 천문 양자 간섭계의 일치율은 양자화 축의 방향으로 양의 및 음의 속도 성분을 가진 광자 궤적 사이의 상대적으로 큰 사소한 기하학적 위상 차이로 인해 순수한 양자 광학 효과 인 Hong-Ou-Mandel dip과 함께 변할 수 있음을 보였다.

주요어: Wigner 회전, 천문 간섭계, QKD, Hong-Ou-Mandel 효과

학번: 2017-31651